

## The Representation of Water Vapor and Its Dependence on Vertical Resolution in the Hadley Centre Climate Model

V. D. POPE, J. A. PAMMENT, D. R. JACKSON, AND A. SLINGO

*Hadley Centre for Climate Prediction and Research, Met Office, Bracknell, Berkshire, United Kingdom*

(Manuscript received 26 April 2000, in final form 22 November 2000)

### ABSTRACT

Simulations of the Hadley Centre Atmospheric Climate Model version 3, HadAM3, are used to investigate the impact of increasing vertical resolution on simulated climates. In particular, improvements in the representation of water vapor and temperature in the upper troposphere and lower stratosphere are identified with more accurate advection. Degradations in some aspects of the simulation in the Tropics are identified with undesirable resolution dependencies in the physical parameterizations. The overall improvements in the water vapor and temperature distribution lead to improvements in the clear-sky longwave radiative fluxes with higher vertical resolution.

### 1. Introduction

Water vapor is one of the key components of the climate system. It is integral to the hydrological cycle and affects the radiative balance of the atmosphere, both directly through clear-sky fluxes and indirectly through cloud forcing. However, water vapor is difficult to model accurately in a general circulation model (GCM), since it depends on modeling adequately both the resolved advection, parameterized advection in such processes as convection and the various changes of phase inherent in the model's physical parameterization schemes. Particular areas of difficulty are the tropopause region, where vertical advection is inaccurate because of the change from relatively moist air in the troposphere to very dry air in the stratosphere, and the Tropics, where convection is important. Evaluating this aspect of model performance has also been a problem in the past, since accurate global three-dimensional analyses of water vapor were not available. In this paper we make use of a state-of-the-art climate model—HadAM3, the atmospheric component of the Hadley Centre climate model (Pope et al. 2000), part of the Met Office's Unified Model (UM)—and some of the best observations and analyses currently available. We highlight the problems of modeling water vapor and demonstrate the benefit of one possible improvement, namely increasing vertical resolution.

Continually improving technology means that climate

modelers need to plan ahead on how they will use increased computing power, as it becomes available. The most obvious ways of using it are (a) to increase the length and number of integrations, (b) to use more computationally expensive formulations, and (c) to run models at higher resolution. Climate modelers tend to use a combined approach. Option (a) is attractive because it means that more reliable statistics will be available from the results (for recent examples using the Hadley Centre model see studies by Rowell 1998; Collins et al. 2001). However, this needs to be balanced by the requirement that physical processes are adequately represented—hence the need for options (b) and (c). A number of projects are aimed at improving the physical parameterizations of the UM and these are reported elsewhere—that is, a new microphysically based precipitation scheme (Wilson and Ballard 1999) and a new boundary layer scheme (Martin et al. 2000). These impact on water vapor as well as other components of the climate system. Stratton (1999) reported the impact of increasing horizontal resolution in a previous version of the model, HadAM2b, and a more comprehensive study of the sensitivity of HadAM3 to increased horizontal resolution is in preparation. These show an improved climatology with increased resolution. However, the cost is high and the improvements in water vapor are marginal. For this reason, we concentrate in this paper on the impact of increasing vertical resolution.

A number of studies over the last decade are relevant to the choice of levels in general circulation models. There are very few studies, however, that have looked systematically at the impact of changing resolution in climate models with a full representation of physical processes and none that have focused on the impact on

---

*Corresponding author address:* Dr. Vicky D. Pope, Hadley Centre for Climate Prediction and Research, Met Office, London Road, Bracknell, Berkshire RG12 2SY, United Kingdom.  
E-mail: vicky.pope@metoffice.com

water vapor. Some studies focus on accurately representing atmospheric waves. For example Lindzen and Fox-Rabinovitz (1989) suggest that consistent horizontal and vertical scaling is needed to represent atmospheric waves accurately, and avoid noise in simulations. Their argument is based on the Rossby ratio between horizontal and vertical scales in quasigeostrophic flow and the dispersion relation for internal gravity waves. The consistency requirements vary with latitude and wave class so it is not possible to construct a fixed resolution model on this basis. This study does not take into account the resolution requirements of other physical processes. Near the equator, for example, Nigam et al. (1986) show that nonlinear processes smooth fields naturally so as to diminish vertical resolution requirements. Ji and Baer (1992) use a series of experiments of varying horizontal resolution with an adiabatic version of the National Center for Atmospheric Research community climate model (CCM0) to show that a nonlinear dynamical model that is consistently truncated may achieve improved results.

Other studies have concentrated on the impact of vertical resolution on the physical parameterizations used in climate models. For example, Lane et al. (2000) and Tompkins and Emanuel (2000) use single-column models to investigate the sensitivity of various physical processes and parameters to changes in vertical resolution. This approach has the advantage of being cheap to run and both studies include results for a wide range of resolutions. A further advantage of this approach is that it allows model sensitivities to be detected in the model's equilibrium state without the complication of large-scale dynamics. This can in itself be a disadvantage since the feedback with dynamics can be an important part of the global model's response. Another problem with single-column tests is that they represent an equilibrium state and do not allow realistic feedback, even ignoring the dynamical feedback. Also, they may not be representative of realistic model states.

Early studies of GCM sensitivity to resolution (WMO 1987) show improved large-scale model performance of numerical weather prediction models with increased vertical resolution. Mahlman and Umshied (1987) claim to represent gravity waves in the Geophysical Fluid Dynamics Laboratory SKIHI model with a vertical resolution of 1 km. However, Lindzen and Fox-Rabinovitz (1989) point out that even this resolution will not be adequate near critical surfaces, which may affect the gravity wave structure at all levels and may account for the noise in Mahlman and Umshied's results. Boville (1991) shows that CCM1 with a horizontal resolution of T21 is not sensitive in the extratropics to an increase in vertical resolution from 1.5 to 0.75 km. He points out that this is not surprising since 1.5 km is adequate to represent Rossby wave structures with T21 horizontal truncation. However, he also finds no evidence that inconsistent resolution in the horizontal and vertical results in noise in the simulations. Baer and Zhu (1992)

use CCM1 to show that it is important to choose carefully where the levels are placed for representing the baroclinic modes accurately. Williamson et al. (1998) also stress the importance of choosing the position of levels carefully. They show that the Eulerian approximations in CCM3 are prone to grid-scale noise that can be reduced by making sure the vertical grid varies smoothly with increasing height. This paper together with a companion paper by Williamson and Olsen (1998) compare semi-Lagrangian and Eulerian versions of CCM3 at different resolutions. They find that a colder tropical tropopause in the semi-Lagrangian model results from inadequate vertical resolution of vertical advection. Although the Eulerian model is less sensitive to resolution in the Tropics, the simulation in this region is improved in both models because the convection scheme behaves better with higher resolution. In summary, the available evidence suggests that increasing vertical resolution is likely to improve climate simulations provided the model used is not deficient in other respects (note, e.g., that Boville found no noticeable improvement in his T21 model) and the level spacing is chosen carefully.

The experiments reported here are Atmosphere Model Intercomparison Project number 2 (AMIP2) 17-yr integrations forced with observed sea surface temperatures, one with the standard 19-level version of HadAM3 (L19) and the other with a higher vertical resolution 30-level version (L30). AMIP2 provides a standardized atmosphere-only climate integration forced with observed sea surface temperatures and a standard ozone dataset as outlined by Gleckler (1996). An ensemble of six L19 integrations and four L30 integrations have been performed. We have used these to check that all the differences between the L19 and L30 integrations that we report are outside the internal variability of the model. The Hadley Centre model is a gridpoint model with Eulerian advection and a horizontal grid of  $2.5^\circ \times 3.75^\circ$ . It uses 19 levels from the surface to the mid-stratosphere. This horizontal and vertical resolution is typical of most climate models. Based on the scaling arguments of Lindzen and Fox-Rabinovitz (1989) the vertical resolution of roughly 2 km in the free troposphere is inadequate to represent atmospheric waves accurately. Increasing the number of levels to 30 increases the resolution in the free troposphere to 1 km, which is more appropriate for the scales of motion represented on the horizontal grid at midlatitudes. Both sets of levels have been carefully tested and tuned to ensure that they are smooth enough to avoid the noise problems pointed out above. Most of this testing was done in the version of the UM used for numerical weather prediction (see, e.g., Milton et al. 1998). The levels correspond to those used in the old (L19) and current (L30) versions of the Met Office numerical weather prediction models.

On increasing vertical resolution in HadAM3 we find dramatic improvements in water vapor and other basic fields such as temperature. The results also highlight

some inadequacies in the model's physical parameterizations. This is an example of how testing a model in different configurations can aid model development by drawing out model deficiencies that are not obvious in a single configuration. Such testing is at the heart of the development of the UM, which is one of the few GCMs used for both climate modeling and weather forecasting. While the detailed resolution sensitivity is particular to the Hadley Centre model, the philosophy and method of analysis is relevant to other climate models. Also, comparison of resolution sensitivity in different climate models will provide another method of comparing climate models over and above the basic AMIP2 comparisons. Indeed, the experiments reported in this paper form part of a set of resolution sensitivity experiments performed with HadAM3 for the AMIP2 subproject on resolution.

The paper is organized as follows. In section 2 we describe the model and analyses used to evaluate it. In section 3 we describe the statistically significant changes in the model climatology. In section 3a we evaluate model performance, identifying improvements and degradations of a range of basic model fields against climatologies. In section 3b we highlight the improvements in the mean water vapor fields around the tropopause, by comparing our results with data from the Halogen Occultation Experiment (HALOE) on the *Upper Atmosphere Research Satellite (UARS)*. In section 4 we investigate the physical processes responsible for these changes. In particular, we quantify the impact of individual physical parameterizations on the temperature and water vapor. We also examine the effect of water vapor and temperature on the radiative balance. Finally, section 5 contains our conclusions.

## 2. Model and analyses

### a. Model

This study uses the latest version of the Hadley Centre climate model, known as HadAM3. Pope et al. (2000) give details of the components of this model together with an analysis of the model's climatology. Model schemes are summarized in appendix A. The model levels used in the two experiments are illustrated in Fig. 1. The standard 19 levels are those used currently in all atmospheric and coupled climate simulations. The higher-resolution 30 levels are those being used in the latest version of the operational forecast model and being tested for the next version of the climate model. The top three and bottom three levels are the same in the L19 and L30 integrations, with the extra levels distributed roughly equally inbetween. The L19 results are for a six-member ensemble and the L30 results for a four-member ensemble. The ensemble members were initialized from model dumps in successive Decembers. The statistical significance of differences between the L19 and L30 ensembles have been assessed using the

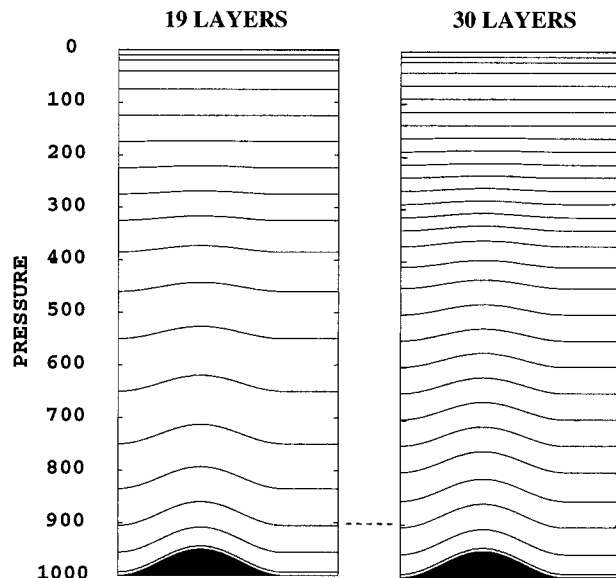


FIG. 1. Arrangement of model levels in the L19 and L30 configurations of HadAM3.

method outlined in appendix B and only differences significant at the 95% confidence level are plotted.

### b. Climatologies used for model evaluation

#### 1) ERA

We make extensive use of the European Centre for Medium-Range Weather Forecasts (ECMWF) reanalysis (ERA) climatology (Gibson et al. 1997; Kallberg 1997) for evaluating the basic model fields. We also use retrievals of water vapor from the HALOE instrument. Work is underway in the Hadley Centre to provide a direct simulation of the satellite radiances from within the climate model (M. Ringer 2000, personal communication). In future studies, we also intend to compare the upper-tropospheric water vapor from the model with the latest retrievals obtained from the Microwave Limb Sounder (Stone et al. 2000) on *UARS*. The ERA dataset has certain advantages for evaluating climate models, however, Pope et al. (2000) discuss some of these, together with the disadvantages. The particular advantages for evaluating model water vapor are outlined in the following discussion.

There is no doubt that it is difficult to obtain accurate water vapor analyses for evaluating models. Radiosonde observations are sparse in some regions and satellite observations do not contain complete information on the vertical profile. In ERA, global radiosonde observations and Television Infrared Observation Satellite (TIROS) Operational Vertical Sounder (TOVS) radiances over the tropical oceans are combined with model information using one-dimensional variational data assimilation, 1DVAR (McNally and Vesperini 1996). This has the advantage of making best use of all the available

information via a model, but the disadvantage that it contains model information (and therefore is influenced by model errors). McNally and Vesperini (1996) showed that the column water vapor obtained using 1DVAR compared well with independent Special Sensor Microwave/Imager (SSM/I) measurements. They also showed that the analyses are not strongly dependent on the characteristics of the model used. The value of the reanalysis approach is that it performs a forward simulation of the radiances from the model and minimizes the differences by adjusting the model fields, so it effectively performs a dynamic retrieval that optimizes the use of the information in both the radiances and model fields. The water vapor distribution is determined by physical processes (such as convection and advection) in the atmosphere and the model provides a link between these processes and the observations to determine the analyzed fields. For example, there is a strong correlation between the upper-tropospheric water vapor distribution and the divergent circulation (see, e.g., Plate 2 of Stone et al. 2000). Improved analysis of the divergent circulation can thus help improve the analysis of specific humidity,  $q$ , and vice versa. By evaluating the model against ERA, the model deficiencies in one field can be easily related to deficiencies in another field. For example, errors in the water vapor distribution are related in part to errors in advection.

The ERA dataset also provides information on the vertical structure of water vapor in the troposphere in a form that can easily be compared with the model, that is, mixing ratios on a pressure grid. It is important to realize that the vertical resolution of the resulting water vapor analysis is ultimately controlled by the radiances. In order to demonstrate that the vertical structure provided by ERA is useful, we have made a preliminary comparison of ERA water vapor in different layers with corresponding layers in the National Aeronautics and Space Administration (NASA) Water Vapor Project (NVAP) dataset (Randel et al. 1996). The two datasets use similar sets of observations but analyze the data in very different ways, thus providing partially independent datasets. NVAP combines radiosonde humidities, satellite water vapor retrievals from TOVS and SSM/I weighting the data according to the perceived reliability of each observing system (with no model information). Our results (not shown) indicate that where the datasets disagree, this can be accounted for by known problems in the individual observing systems used in NVAP (Randel et al. 1996).

## 2) CMAP

Precipitation is evaluated against the Climate Prediction Center (CPC) Merged Analysis of Precipitation (CMAP; Xie and Arkin 1997). This is a global, monthly precipitation dataset covering the 17-yr period 1979–95. It incorporates gauge observations and estimates inferred from a variety of satellite observations.

## 3) ERBE

Satellite measurements of radiative fluxes made between 1985 and 1990 by the Earth Radiation Budget Experiment (ERBE) (Harrison et al. 1990) are used to evaluate the model's radiation fluxes at the top of the atmosphere.

## 4) HALOE

One of the areas we particularly highlight is the improvement in upper-tropospheric and lower-stratospheric water vapor. The quality of the ERA water vapor analyses in this region is less reliable (particularly in the lower stratosphere) because there are so few measurements and the analyses do not assimilate any water vapor observations in the stratosphere. The ERA climatology used here sets water vapor to  $2.5 \times 10^{-6}$  kg kg<sup>-1</sup> (3.88 ppmv) at stratospheric levels, or to the saturation mixing ratio if that is lower. Note, however, that ECMWF have recently abandoned this practice and now use analyzed values of water vapor in the stratosphere (Simmons et al. 1999). However, observations of water vapor in the upper troposphere–lower stratosphere have been made by the HALOE instrument (Russell et al. 1993) that flies on *UARS*. This dataset is thus a very useful tool for validating the model water vapor in the upper-troposphere–lower-stratosphere region.

HALOE is a solar occultation instrument; observations are made twice a day, at sunrise and sunset, and are clustered round two rings of latitude (one for sunrise, one for sunset). As the orbit drifts these latitudes slowly change, and thus it takes a few weeks to build up global coverage. For most of the year the observational domain is restricted to the 45°S–45°N band. HALOE water vapor retrievals extend from near the tropopause to approximately the 0.002-hPa level with a vertical resolution of about 2 km and an accuracy of  $\pm 10\%$  between 100 and 0.1 hPa, rising to  $\pm 30\%$  at the boundaries of the observational range (Harries et al. 1996). HALOE cannot observe deep into the troposphere, because of high absorption and scattering, but it provides a useful means of assessing model performance near the tropopause and in the lower stratosphere. The HALOE seasonal means presented here have been calculated using observations from December 1992 to February 1997 (i.e., they do not coincide exactly with the AMIP2 period). The accuracy of the HALOE data means that we can use them to evaluate three-dimensional structure in the lower stratosphere but only zonal-mean structure in the upper troposphere.

## 3. Results

### a. Mean fields

#### 1) TEMPERATURE AND MOISTURE

The most significant changes in model climatology when the resolution is increased from 19 to 30 levels

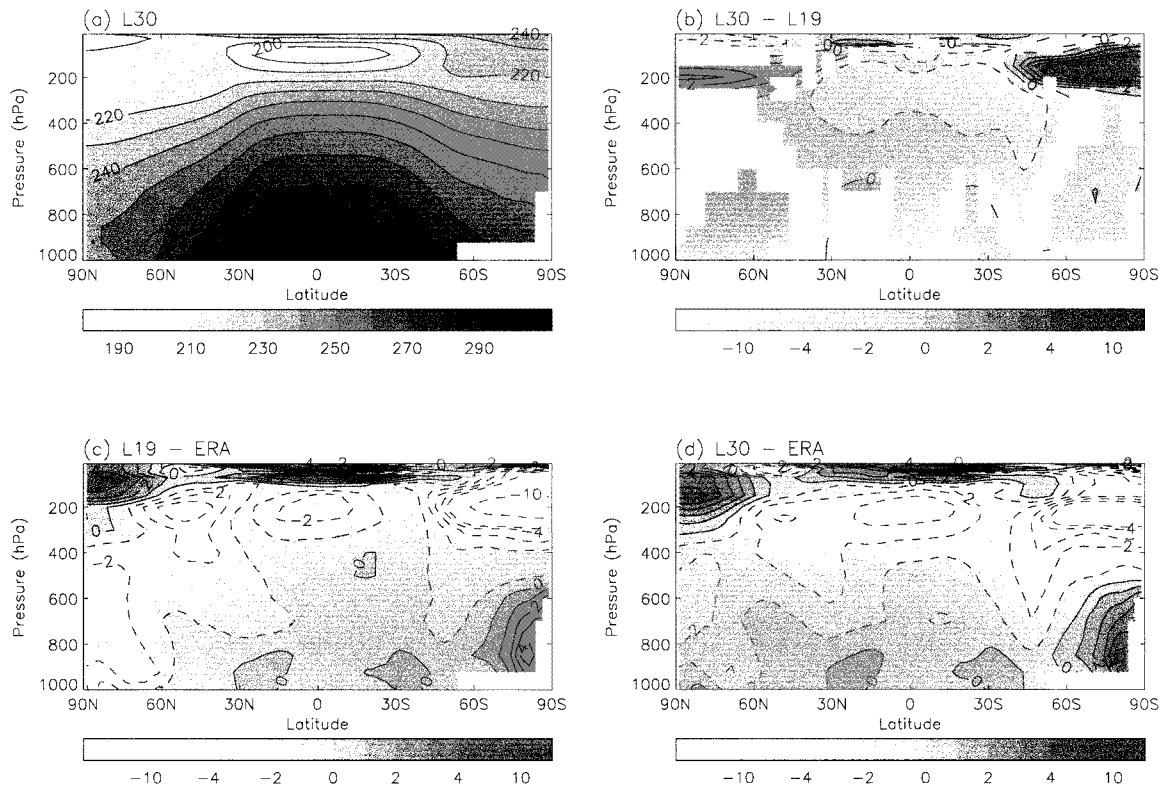


FIG. 2. Lat–pressure cross sections of zonal-mean temperature. The 17-yr DJF mean from 1979 to 1995 for model data and 15-yr mean from 1979 to 1993 for climatological data as follows. L30 fields are the means of a four-member ensemble and L19 fields are the mean of a six-member ensemble. (a) L30, (b) L30 – L19—only differences significant at the 95% confidence level are plotted, (c) L19 – ERA, and (d) L30 – ERA. The contour interval is 10 K in Fig. 2a and irregular contours as indicated in the key in the other panels.

are in the temperature and humidity fields. The impact on temperature is shown in Fig. 2 together with differences between the models and the ERA climatology. In common with many GCMs all recent versions of the Hadley Centre model have a cold bias in most of the troposphere. Reductions in this bias have come about through the inclusion of a new radiation scheme (Pope et al. 2000; Edwards and Slingo 1996). Figure 2 shows that in the L30 model there is a further substantial reduction in the cold bias in the upper troposphere at mid- and high latitudes. For example, temperatures above 200 hPa near the South Pole increase as much as 7 K even in the mean, reducing the coldest bias from 13 to 7 K. The main degradation is that the cold bias is increased in the tropical upper troposphere from 2 to 3 K. In section 4 it is shown that the improvements in temperature climatology largely come about through improved representation of the dynamics. The more mixed changes in the Tropics arise from resolution dependencies in the physical parameterizations in the model.

Figures 3 and 4 show relative and specific humidity. In the L19 model there is a large moist bias in the extratropics (particularly striking in terms of relative humidity in the upper troposphere) and a weak dry bias in the Tropics. In the L30 model the moist bias is substantially reduced in the extratropical upper troposphere.

Decreases in specific humidity and increases in temperature are linked to a reduction in relative humidity of up to 20% around 200 hPa and a reduction in the maximum moist bias from 45% to 35%. Similarly, in the tropical lower stratosphere (around 100 hPa) increases in specific humidity and decreases in temperature are linked to an increase in relative humidity of up to 10%, thus halving the dry bias in this region. The reduction in errors is encouraging. However, we must be careful using ERA analyses in these regions since above the tropopause specific humidity is set to 2.5 mg kg<sup>-1</sup> or the saturation specific humidity, whichever is lower. Ovarlez and van Velthoven (1997) noted that ERA values of moisture were spuriously dry in the lower stratosphere when compared with aircraft measurements. Hence the dry bias in our model is probably larger than suggested by comparison with ERA. In section 3b we use HALOE observations to make a more accurate assessment of our results. Notice that in both the extratropical upper troposphere and tropical lower stratosphere the specific humidity does not appear to be responding to changes in temperature, since we might expect a colder (warmer) atmosphere to hold less (more) moisture and the opposite is true. This point will be picked up later when we discuss how these changes occur.

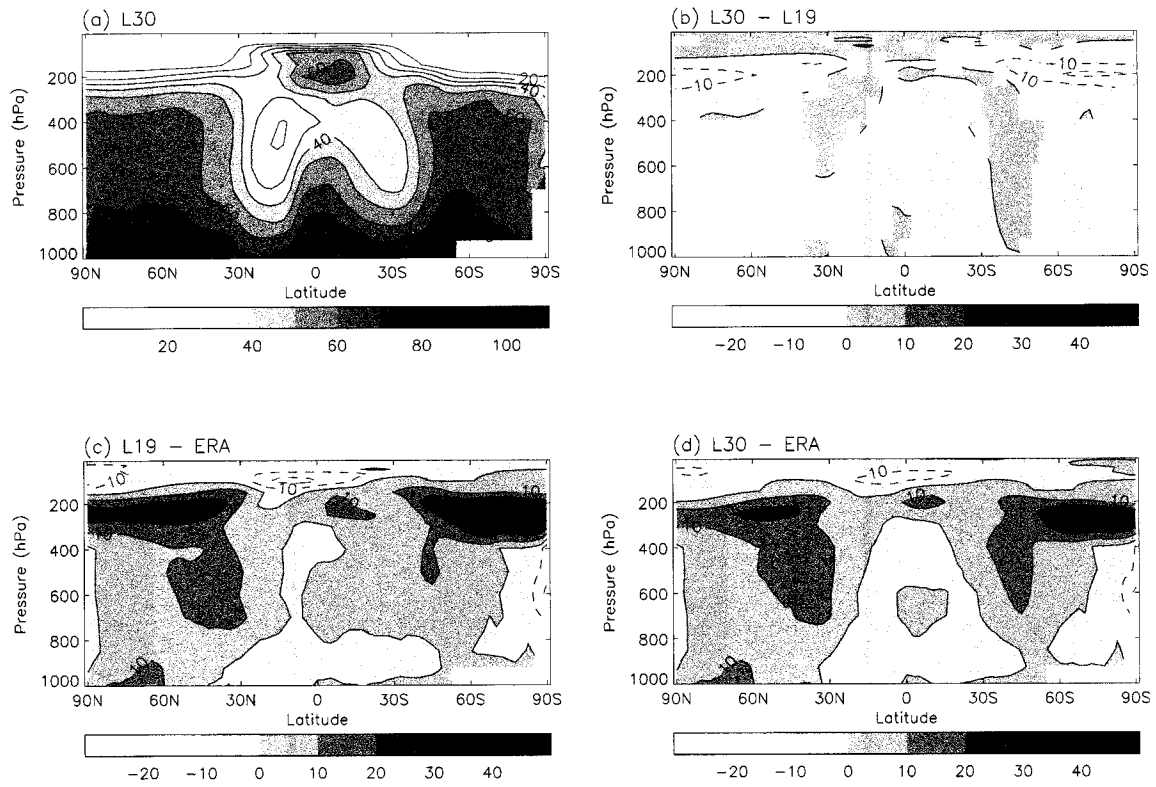


FIG. 3. As Fig. 2 but for zonal-mean relative humidity. The contour interval is 10%.

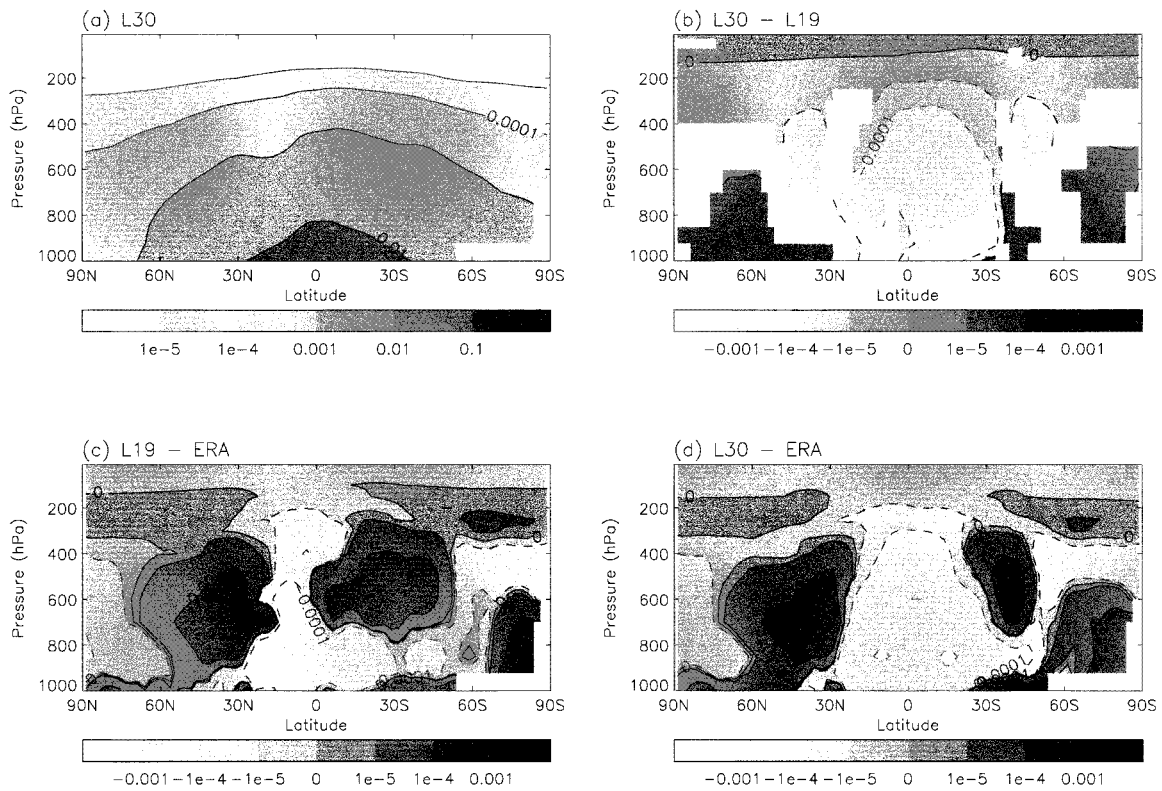


FIG. 4. As Fig. 2 but for zonal-mean specific humidity,  $q$ . The units are in  $\text{kg kg}^{-1}$  and contours are evenly spaced in  $\log q$ , i.e.,  $10^{-5}$ ,  $10^{-4}$ , ...,  $0.1$  in (a) and  $-10^{-3}$ ,  $-10^{-4}$ ,  $-10^{-5}$ ,  $0$ ,  $10^{-5}$ ,  $10^{-4}$ ,  $10^{-3}$  in (b)–(d).

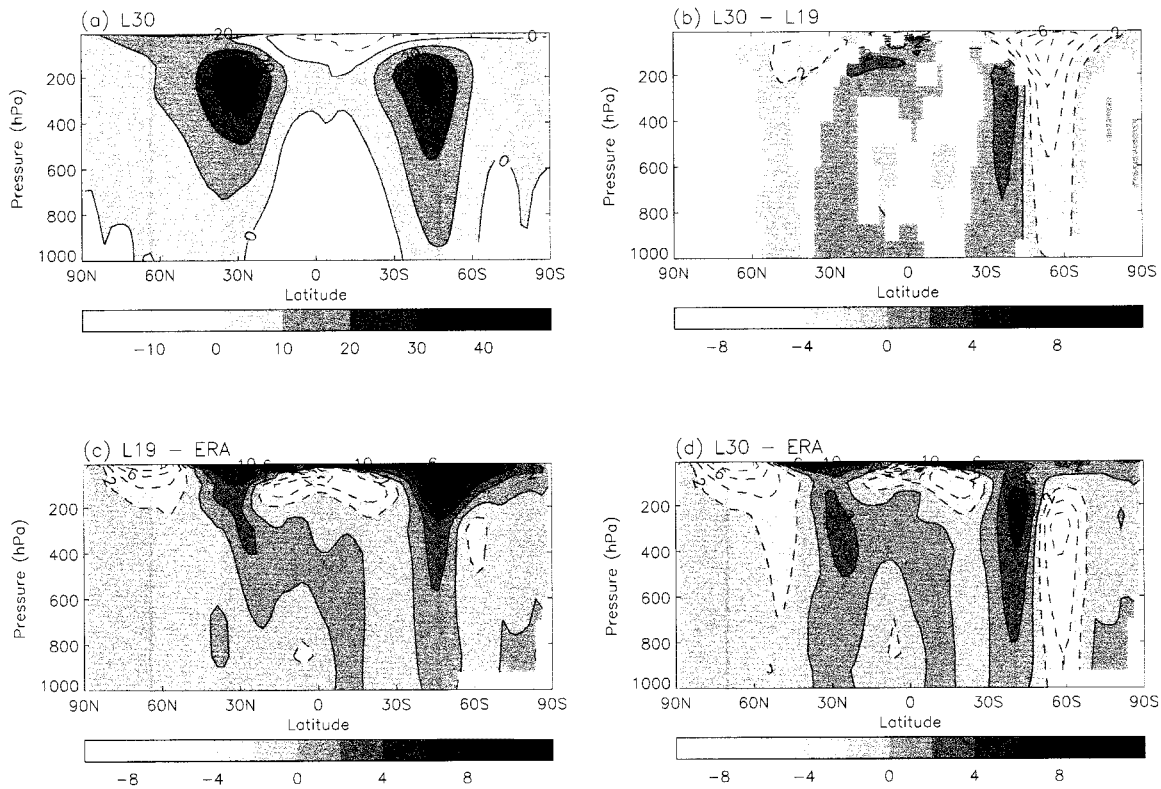


FIG. 5. As Fig. 2 but for zonal-mean zonal wind. The contour interval is  $10 \text{ m s}^{-1}$  in (a) and  $2 \text{ m s}^{-1}$  in (b)–(d).

In contrast, in the mid- and lower troposphere temperature decreases (increases) tend to go hand in hand with specific humidity decreases (increases). In the extratropics the temperature changes tend to dominate the relative humidity response. For example, between  $30^\circ$  and  $60^\circ$  temperature and specific humidity decrease and relative humidity increases, increasing maximum errors from 10% to 15%. In the Tropics, on the other hand, the specific humidity changes dominate. At the equator relative humidity decreases by 5% increasing errors from close to 0% to 5% due to sensitivities of the model parameterizations (section 4). These results are consistent with the findings of Peixoto and Oort (1996), who found that relative humidity in the atmosphere is primarily determined by temperature in the extratropics and specific humidity in the Tropics.

## 2) CIRCULATION

Changes in the mean circulation at mid- and high latitudes are consistent with changes in the temperature structure. Figure 5 shows the zonal mean wind. The midlatitude westerly jets are decreased in strength, particularly on their poleward flank. The changes are consistent with the reduced horizontal temperature gradients. Also, the jet shifts slightly equatorward. In the Northern Hemisphere changes in zonal mean wind are small (up to  $2 \text{ m s}^{-1}$ ). The only detrimental impact is

the equatorward shift of the jet. There is also an associated equatorward shift of the storm tracks, degrading the simulation (currently under investigation). In the Southern Hemisphere changes are larger and extend from the surface (up to  $2 \text{ m s}^{-1}$ ) into the stratosphere (up to  $8 \text{ m s}^{-1}$ ). The westerly bias above 200 hPa is virtually removed, although the easterly bias poleward of  $40^\circ\text{S}$  below 200 hPa is increased. This pattern of response in the Southern Hemisphere is very like the so-called annular mode (see, e.g., Thompson and Wallace 2000). Similar impacts on the jet structure come from changing the dynamics time step, suggesting a dynamical cause for the signal. In the Tropics changes in the circulation are generally small and few are statistically significant. The easterly bias around 200 hPa just north of the equator is reduced slightly (by  $2 \text{ m s}^{-1}$  at the most). There is also a slight weakening of the Hadley circulation, and it does not extend as far into the stratosphere (see Fig. 12 in section 4a).

## 3) PRECIPITATION

It is important for a climate model to have a reasonable representation of surface fields such as precipitation. The impact of increasing resolution on precipitation is not direct and is therefore very complex in the model. Any degradations in the simulation do not necessarily indicate that high resolution is inappropriate,

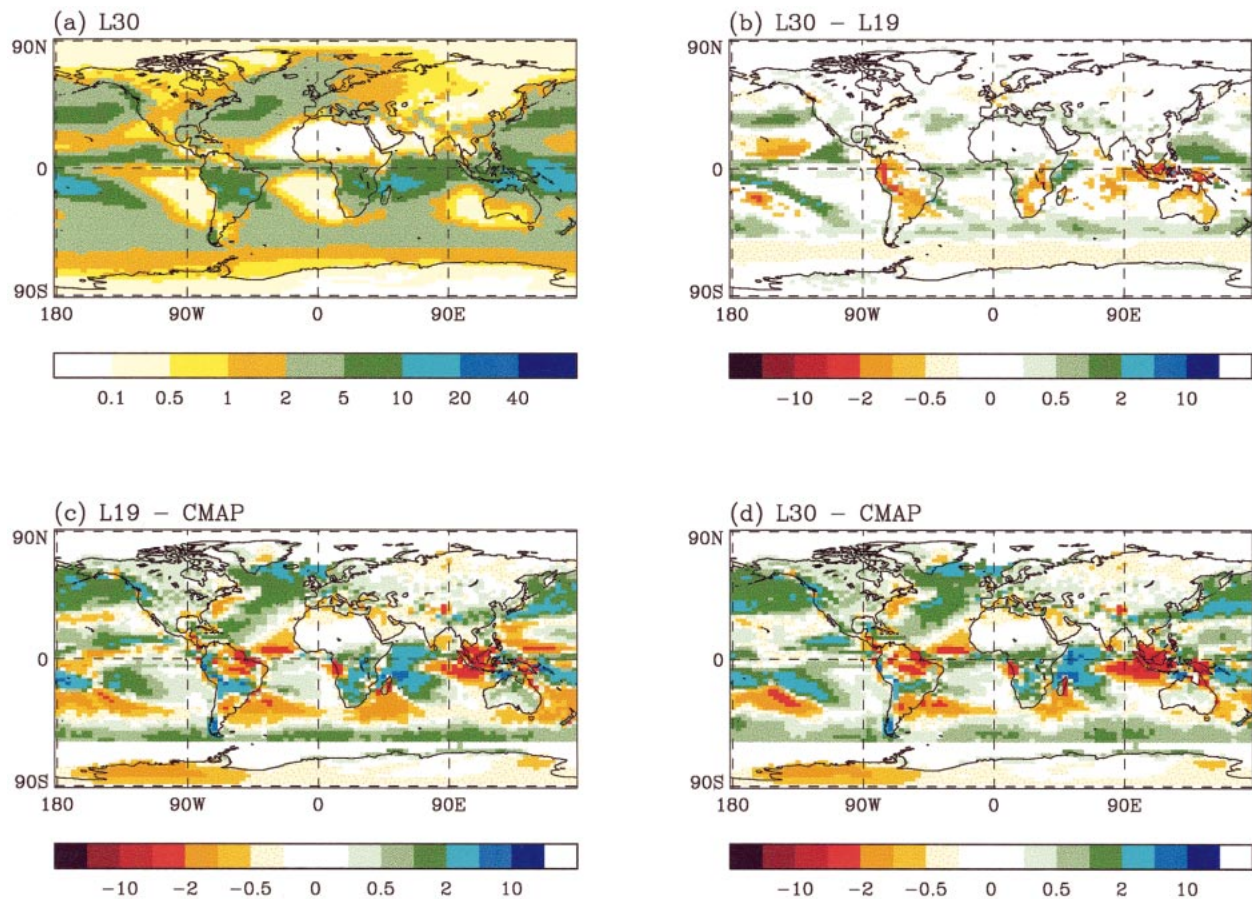


FIG. 6. As Fig. 2 but lat–long plot of precipitation evaluated against the CMAP climatology (Xie and Arkin 1997). (Units:  $\text{mm day}^{-1}$ .) The plots use an uneven scale defined in the key.

but may point to sensitivities in the model parameterizations that need to be investigated further. A study of the impacts on precipitation can start to give some insight into how the physical processes in the model are altering with increased resolution, since precipitation changes in response to changes in such processes as convection and resolved convergence.

Figure 6 shows that there is good agreement between the precipitation in HadAM3 and in the CMAP dataset. When vertical resolution is increased, precipitation in the Tropics decreases in the convectively active regions and shifts to the less active regions. Over tropical land, in particular to the south of the equator, precipitation decreases by over  $2 \text{ mm day}^{-1}$  in places, improving agreement with CMAP. Over tropical sea, precipitation increases in most places. Rainfall shifts from the Maritime Continent (worsening agreement with climatology) to the northeast over the Pacific (improving agreement with climatology). These changes in precipitation are consistent with changes in convective heating locally (see section 4 for further discussion) confirming that changes in convection are associated with changes in precipitation. This is to be expected since convection dominates the modeled precipitation in the Tropics. In

the extratropics we noted that the jet shifts equatorward (Fig. 5) associated with an equatorward shift in the storm tracks. Correspondingly, precipitation decreases on the poleward flank of the storm tracks and increases on the equatorward flank. The decreases in the Northern Hemisphere are not statistically significant, however, because of the large variability in the Northern Hemisphere winter storm tracks.

#### b. Water vapor in the tropopause region

One of the major benefits in increasing the vertical resolution of the model is in resolving the structure of the tropopause more accurately. We would expect improvements in transport in this region to lead to improvements in the water vapor climatology in the model. As already pointed out, the ERA data are not suitable for a detailed evaluation of the model in the tropopause region. Instead, we use observations made by HALOE, which provides independent observations of water vapor in the upper troposphere–lower stratosphere. Figure 7 focuses on specific humidity above 150 hPa comparing the two model versions with HALOE observations. Note that the HALOE seasonal means presented here use ob-

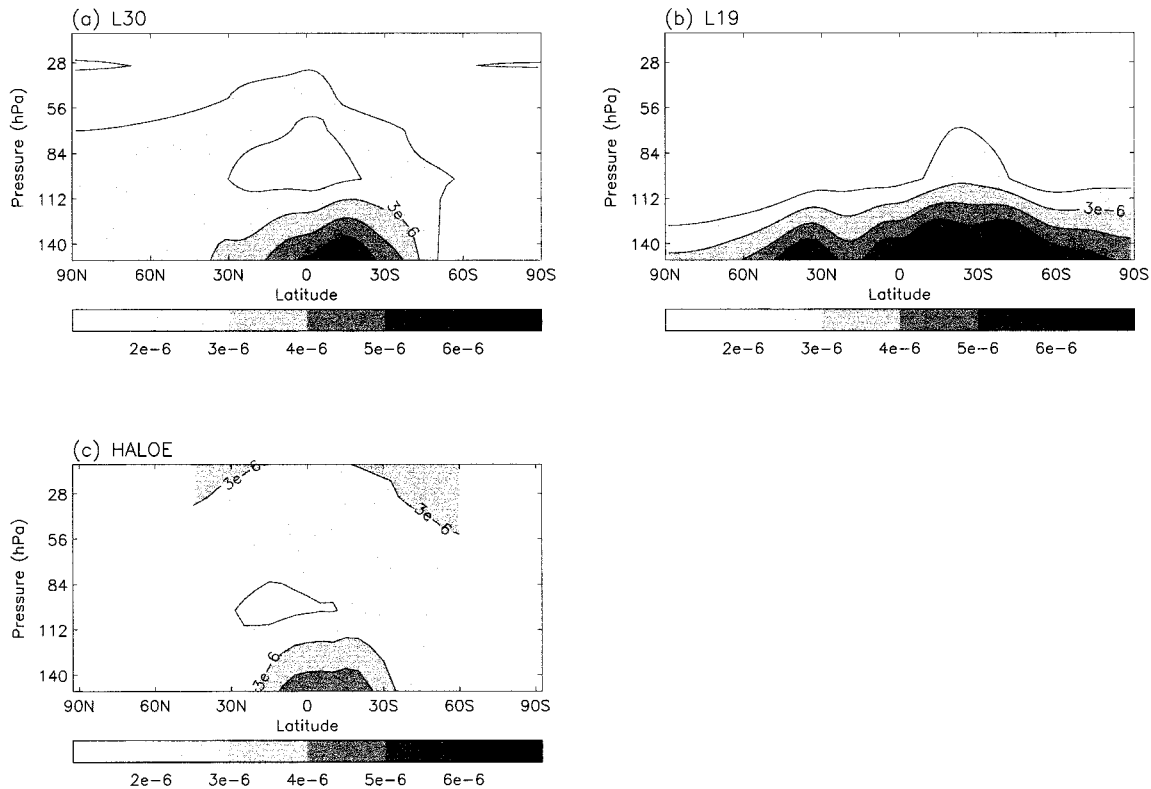


FIG. 7. Lat–pressure cross sections of zonal-mean specific humidity from 150 to 10 hPa for (a) L30 ensemble mean, (b) L19 ensemble mean, and (c) HALOE. Both (a) and (b) are 17-yr DJF means from 1979 to 1995, (c) is a 5-yr DJF mean from 1992 to 1997. The contour interval is  $10^{-6}$  kg kg $^{-1}$ .

servations from December 1992 to February 1997 (DJF) and therefore do not correspond to the AMIP period but overlap for only a couple of years.

At most stratospheric levels above 100 hPa, water vapor increases with height in the HALOE field. This is because of the chemical production of water vapor by oxidation of methane. Such an increase is not seen in the model fields because the models contain no chemical source of water vapor. The decrease of water vapor with height near the tropopause in the L30 model is generally in reasonable agreement with the HALOE fields, whereas in the L19 model this gradient is too strong. The lower-resolution model is more moist up to around the 140-hPa level (at mid- to high latitudes) and up to around the 100-hPa level (at low latitudes) and is drier above these levels. Near the tropical tropopause there is a well-defined water vapor minimum in the HALOE and ERA fields, which is well simulated by the L30 model version, but which does not appear at all in the L19 field. At mid- and high latitudes in the L30 model, the decrease in upper-tropospheric water vapor with height is much less rapid above the 200–150-hPa region than below, whereas in the L19 model the rapid decrease with height continues up until around the 100-hPa level. The consequence of this is that the arched pattern of the hygropause in the HALOE field (higher at low latitudes than at midlatitudes) is quite well re-

produced in the L30 model, whereas the hygropause in the L19 model is at approximately the same pressure level at all latitudes. It is unclear how realistic the L30 simulation is poleward of  $45^\circ$  where there are no HALOE observations in DJF. The HALOE observational range in March–May and September–November is greater than in DJF, and comparison of model and HALOE fields for these seasons suggests that the hygropause does not arch down enough between the subtropics and high latitudes in the L30 model. The high-latitude hygropause is therefore located too high up, but is still more realistic than the hygropause in the L19 model.

### c. Regional variations in water vapor

The simulation of regional variations of the water vapor field near the tropopause also improves when the number of model levels is increased. Jackson et al. (1998) investigated such regional variations using HALOE data. Figure 8 shows water vapor for DJF and JJA very close to the tropical tropopause, at level 25 in the L30 model together with the closest HALOE analysis level, 100 hPa. In DJF the water vapor at 100 hPa is a minimum at low latitudes (Figs. 8a and 8c). This is because the low temperatures at 100 hPa imply very low water vapor saturation mixing ratios and hence very dry air. Temperatures are lowest over the Indonesia–western Pacific

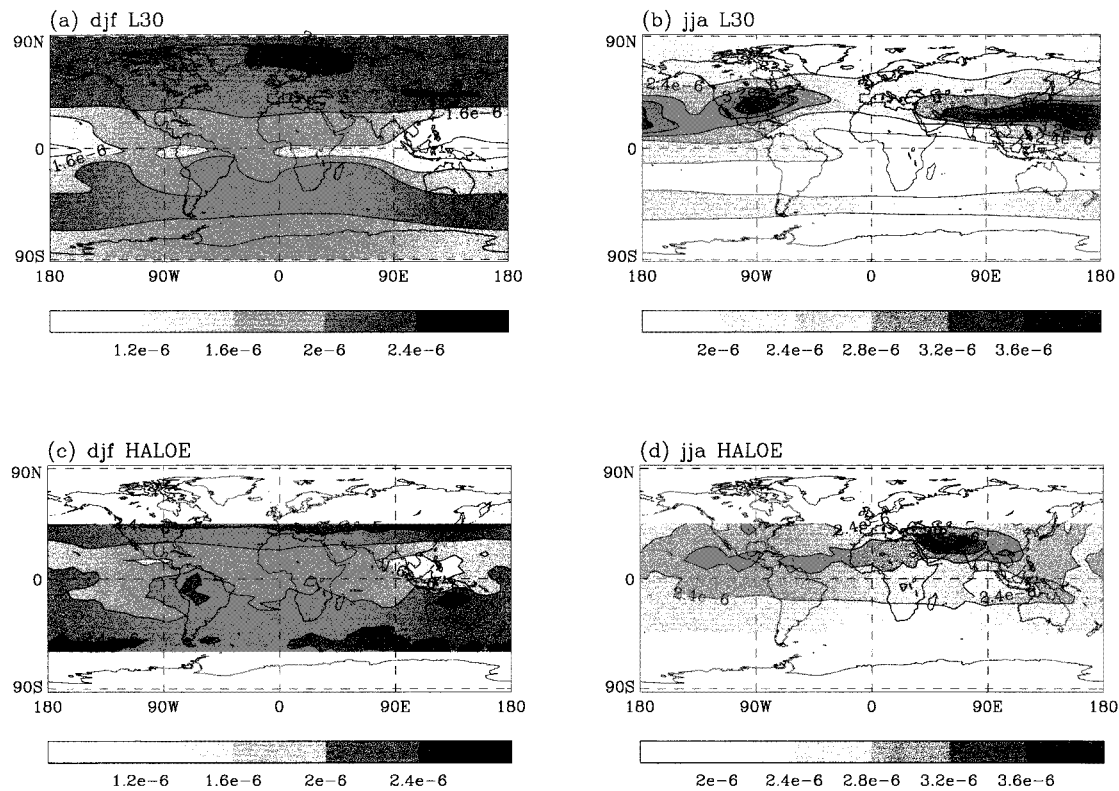


FIG. 8. Lat-long plots of specific humidity for the period used in Fig. 7. (a) L30 level 25, which is roughly equivalent to 102-hPa, DJF mean, (b) as (a) but for JJA mean. (c) As (a) but HALOE data at 100 hPa, (d) as (c) but HALOE data at 100 hPa. The contour interval is  $0.4 \times 10^{-6} \text{ kg kg}^{-1}$ .

region, where convection is strongest, and accordingly water vapor values are lowest near there. The model reproduces this structure quite well, although it is slightly too dry and the dry air is too far east. The error in position arises from errors in the distribution of convection. Notice in Fig. 6d that there is too little precipitation over Indonesia and too much to the east. The model does not have enough water vapor at high latitudes since there is no representation of methane oxidation. There is evidence of this lack at midlatitudes in the Southern Hemisphere at the maximum range of the HALOE data.

Examination of model level fields in the other three seasons shows that, as in DJF, the L30 model fields at level 25 are fairly similar to the HALOE fields at 100 hPa. A particularly striking result from Jackson et al. (1998) is the moistening of the 100- and 128-hPa levels over parts of Asia in JJA, which is associated with the Asian monsoon. The observations for 100 hPa are reproduced in Fig. 8d. There is a similar moistening in the L30 model at level 25 (Fig. 8b). However, the highest values are located farther to the east, being between India and the western Pacific rather than between Saudi Arabia and Southeast Asia. Results from the L30 run are similar to those in Martin (1999), who examined results from an earlier climate version of the UM (which had 19 levels), and showed that the UM simulates the

Asian summer monsoon fairly well. However, the modeled upper-tropospheric tropical easterly jet is stronger than that in ERA, and the shape of the anticyclone located over the Himalaya is also different. In the model it is elliptical and confined close to the Himalaya, while in ERA it is much more elongated and extends west from the Himalaya to the Persian Gulf (see Martin 1999, Fig. 1). Most upward transport of moist air into the upper troposphere and lower stratosphere takes place over the Bay of Bengal–India region. Much of this moist air then gets rapidly advected westward in the real atmosphere, whereas in the model atmosphere much of this air gets transported northward round the western edge of the anticyclone and then rapidly eastward to the Pacific by the subtropical westerly winds. This can explain why the region of moist air is located farther east in the L30 model fields than in the HALOE fields. The importance of advection in determining the horizontal water vapor distribution is demonstrated by the close agreement between moisture fields in Fig. 8 and the corresponding horizontal wind fields (not shown). One point to bear in mind when comparing with HALOE data is that the instrument samples a given region only a handful of times each season. Thus HALOE will not be able to observe properly any short timescale processes that could be important in determining the water vapor distribution in the Asian region. Nor indeed will

it be able to observe properly the active and break periods in the Asian summer monsoon, which have periods between 10–20 days and 30–60 days (see, e.g., Annamalai et al. 1999; Martin 1999).

These fields show that the L30 model is doing a good job of simulating regional variations in the lower-stratospheric water vapor distribution associated with tropical convection. By contrast, the L19 model fails to reproduce most of the observed structure at 100 hPa, producing a structure more similar to the upper troposphere in the L30 model (not shown).

#### 4. Physical processes

##### a. Zonal mean

The impact of increasing vertical resolution on the heating rates for various model schemes are summarized in Fig. 9. Figure 9a shows the impact of increasing vertical resolution on the 17-yr mean temperature. The other panels show changes in the heating rate from various model schemes during an ensemble of 10 3-day “spinup” integrations. Three days is long enough to remove initial noise while still retaining a strong signal of the model drift. Clearly, an ensemble of integrations increases the statistical significance of the results. We have found that 10 are sufficient without being too expensive. These integrations are initialized from analyses for 10 independent days in December. The model drift away from these analyzed states determines the main systematic model errors. This has been confirmed by comparing the pattern of the total spinup heating rate (not shown) with the mean temperature difference. The warming in the extratropics (Fig. 9a) is dominated by increased dynamical heating in the upper troposphere (stretching from 400 hPa at the poles to 200 hPa at 30°N and 30°S in Fig. 9b) and reduced longwave cooling around the tropopause (stretching from 300 hPa at the poles to 150 hPa at 30°N and 30°S in Fig. 9c). The former is discussed in more detail below. The latter occurs because of the reduction in water vapor and cloud in this region (Fig. 4), which leads to reduced longwave cooling to space. Closer examination shows that the clear-sky contribution dominates. The cooling in the Tropics is dominated by increased longwave cooling due to changes in cloud (Fig. 9d, see also section 4b).

Other models do not necessarily show the same sensitivity to resolution. Williamson and Olsen (1998) show (in their Fig. 11) that the tropopause and lower stratosphere cool at high latitudes in the winter hemisphere when vertical resolution is increased in both their semi-Lagrangian and Eulerian models. They do not show changes in water vapor or break down the response of different parts of the model so it is not clear how their results relate to ours. Both their models use semi-Lagrangian advection of moisture and are less affected by the moist bias that dominates our L19 runs; therefore the moisture may be less sensitive to resolution.

Corresponding plots of the water vapor tendencies are shown in Fig. 10. In this case the total water vapor tendency has been included (Fig. 10b). Some of the main features are similar in Figs. 10a and 10b. In particular most of the drying in the Tropics and in the upper troposphere and the moistening in the extratropical lower troposphere and in the stratosphere are seen in both the mean water vapor differences and in the total tendency. The main difference is a moistening in the tropical mid-troposphere, which does not affect the time mean. This moistening comes partly from changes in convective activity (Fig. 10d) and is consistent with the increased detrainment in the midtroposphere identified by Inness et al. (2001) and discussed in section 4b. Figure 10c shows that the upper-tropospheric and stratospheric changes are due to dynamics. They occur, first, because in this region there is a rapid transition from moist tropospheric to dry stratospheric air, and second, because the vertical velocity decreases markedly between the upper troposphere and the lower stratosphere. These two factors are important because the vertical advection term in the prognostic model equation for moisture takes the form

$$1/2 [E_{k+1/2}(q_{Tk+1} - q_{Tk}) + E_{k-1/2}(q_{Tk} - q_{Tk-1})],$$

where  $q_T$  is total moisture (i.e., vapor + liquid + ice),  $E$  is related to the vertical velocity,  $k - 1$ ,  $k$ , and  $k + 1$  refer to full model levels and  $k - 1/2$  and  $k + 1/2$  refer to half levels. (Note that the dynamics scheme advects total moisture, whereas we have diagnosed water vapor in Fig. 10.) With a strong decrease of both vertical velocity and moisture between the upper troposphere and lower stratosphere, the lower the resolution, the more erroneous the advection of moist tropospheric air across the tropopause will be.

In the case of upward motion, high-tropospheric moisture spreads upward. The lack of resolution in L19 means that the high moisture values spread farther upwards and then drop off more rapidly. A good example of this is in DJF (Fig. 7) where the effect of the ITCZ is to transport moist air upward in the southern subtropics. The signature of this is barely perceptible in the HALOE fields, in the L30 model field there is a slight bulge of moister air near 100 hPa and 20°S, whilst in the L19 field this bulge extends up to around 50 hPa (i.e., the next model level above 100 hPa), indicating the way in which low vertical resolution can lead to the smearing of upper-tropospheric patterns up into the lower stratosphere. In the case of downward motion unrealistically low moisture values can be generated above the tropopause with L19, leading in some cases to negative moisture. These are reset to zero by borrowing moisture from adjacent grid points, creating an artificial moisture sink and spreading low values across the layer. This accounts for the very low moisture in the L19 stratosphere (Fig. 7). Strong gradients develop between these very dry layers and the relatively moist upper troposphere.

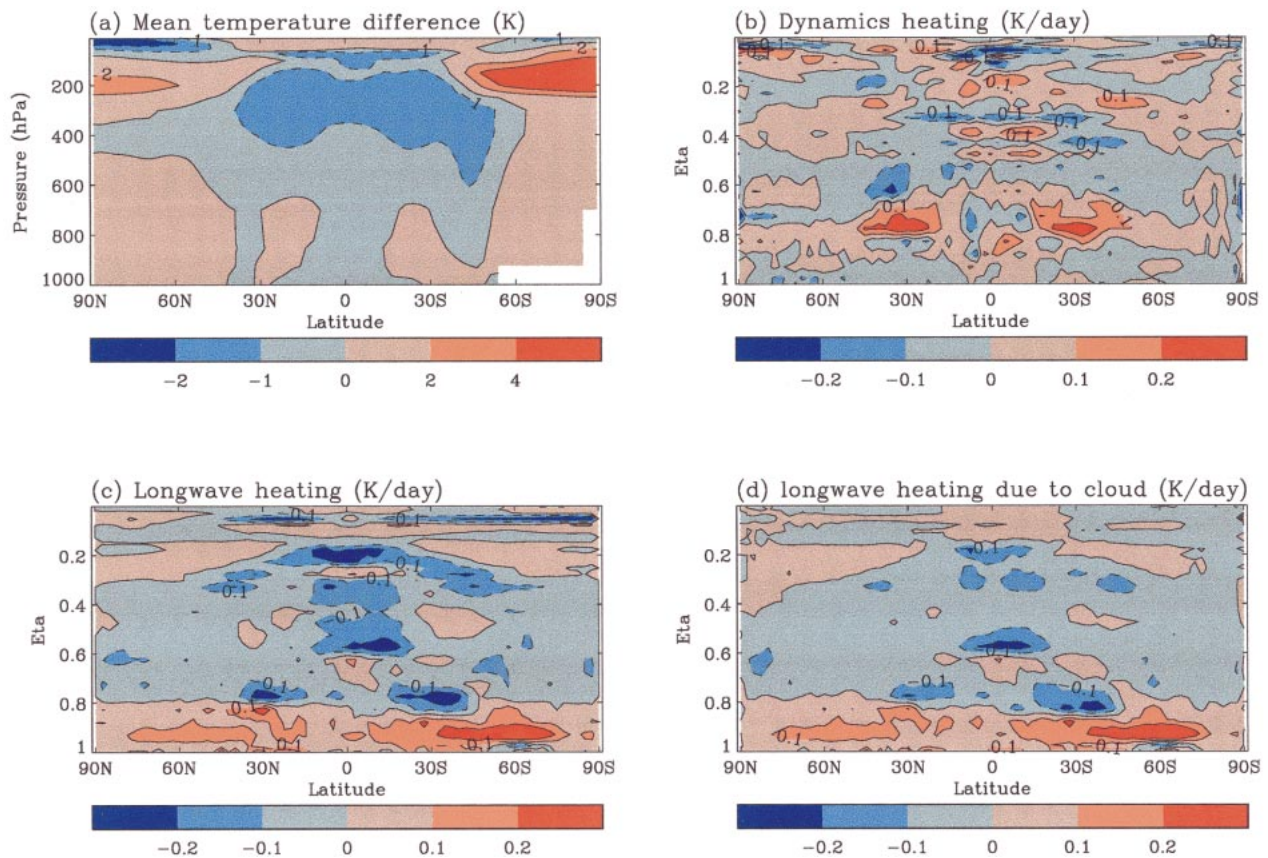


FIG. 9. (a) Lat–pressure cross section of zonal-mean temperature difference between the L30 and L19 ensembles for the 17-yr DJF means from 1979 to 1995. The contour interval is uneven as indicated in the key. (b)–(d) Lat–eta cross section of the zonal-mean heating rate difference between the L30 and L19 models for the mean of ten 3-day spinup integrations initialized from the same set of analyses. Fields are interpolated from model levels to equally spaced eta levels.  $1000 \times$  eta corresponds roughly to pressure. The contour interval is  $0.1 \text{ K day}^{-1}$ .

The variation in vertical velocity with height, illustrated in Fig. 11, accentuates the effects outlined above leading to enhanced upward spread of high-tropospheric water vapor when there is upward motion and more likelihood of negative moisture where there is downward motion. In addition, the Hadley circulation has a slightly greater vertical extent in the L19 model than in the L30 model, and at many latitudes vertical velocities typical of the upper troposphere in the L30 model spread to the lower stratosphere in the L19 model. For example, Fig. 11 shows that in the L30 model the  $-0.001 \text{ hPa s}^{-1}$  contour reaches 100 hPa at low latitudes and is below 150 hPa in southern midlatitudes ( $55^\circ\text{S}$ ), but extends as high as 84 and 120 hPa, respectively, in the L19 model. This also accentuates the difference between vertical advection at the two resolutions.

Further evidence that the very low water vapor in the stratosphere in L19 is numerical and not physically sensible comes from comparing values with minimum saturation vapor pressures in the tropopause region. Figure 12 shows saturation vapor pressure at 100 hPa in DJF. The lowest saturation vapor pressures should determine the lowest water vapor values in the stratosphere since

in reality there are no sinks of moisture in the stratosphere. The lowest saturation vapor pressures arise over Indonesia–western Pacific and these are lower in the L30 model than in the L19 model (minimum values are  $1.4 \times 10^{-6} \text{ kg kg}^{-1}$  for the L30 model and  $2.4 \times 10^{-6} \text{ kg kg}^{-1}$  for the L19 model). These fields are 17-yr seasonal means, but an examination of 12-h fields for one DJF season shows that the temporal variability is sufficiently small that in the L19 model the saturation vapor pressure rarely falls below  $2.2 \times 10^{-6} \text{ kg kg}^{-1}$ . The actual stratospheric specific humidities fall as low as  $0.3 \times 10^{-6} \text{ kg kg}^{-1}$  even in the zonal mean in the L19 model and these values clearly have no physical explanation. In contrast, in the L30 model zonal mean values do not fall below  $1.4 \times 10^{-6} \text{ kg kg}^{-1}$  in the zonal mean consistent with the minimum saturation vapor pressures in Fig. 12.

The increased resolution thus leads to a better representation of the vertical structure and more accurate dynamics in the extratropics. This also accounts for the changes in longwave heating because it is responsible for the reduction in the moist bias. Hence, the improved physical representation in the extratropics leads to an

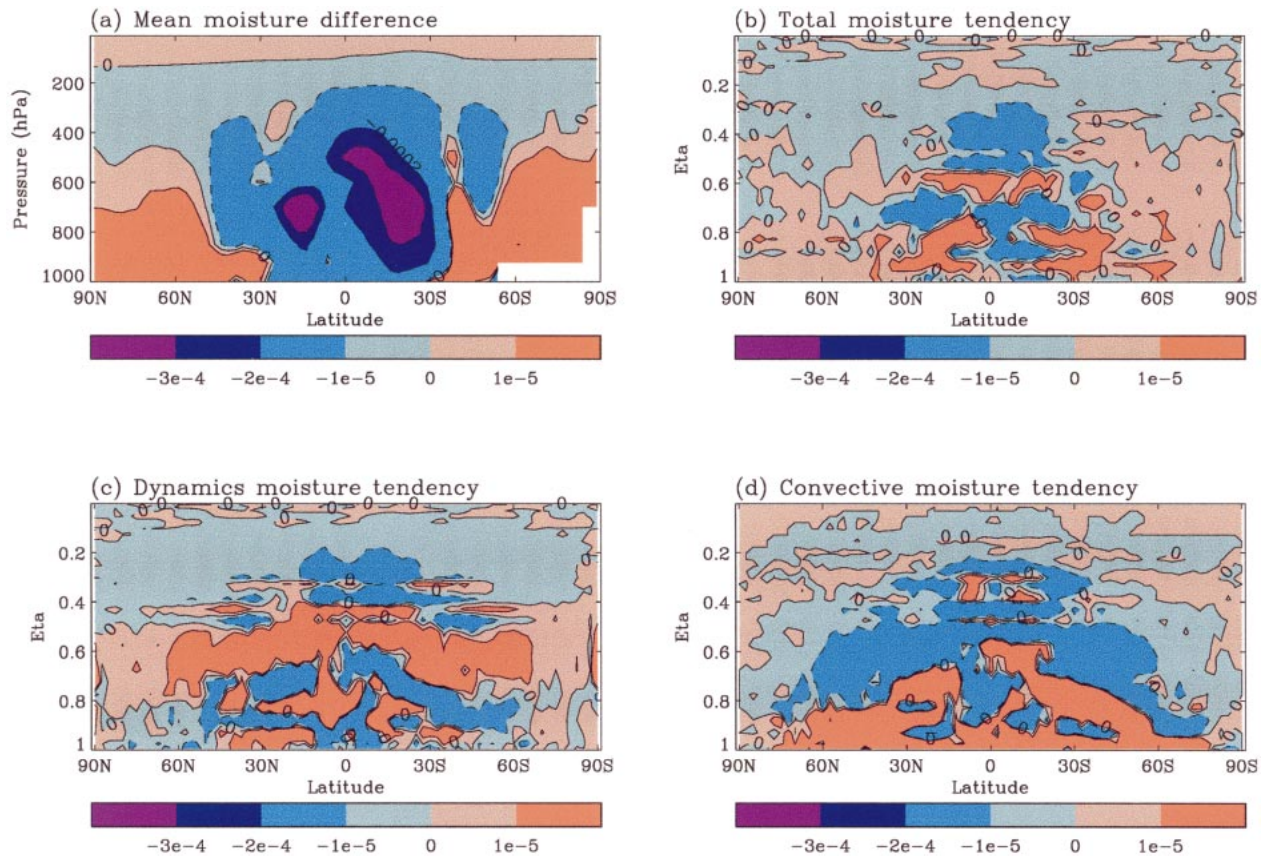


FIG. 10. As Fig. 9 but for specific humidity and its spinup tendency. The units are in  $\text{kg kg}^{-1}$ . The contours are  $-3 \times 10^{-4}$ ,  $-2 \times 10^{-4}$ ,  $-10^{-5}$ , 0,  $10^{-5}$ .

improved climatology. The specific humidity is not simply responding to changes in temperature to maintain the relative humidity (as we pointed out in section 3a), in fact if anything temperature is responding to changes in moisture through longwave heating.

#### b. Local processes in the Tropics

The response of the model to increased resolution is more complex in the Tropics. It involves feedback between the various model schemes. The detailed response is particular to the UM and dependent on the parameterization schemes used. Similar types of feedback are likely in other models, however, and we might learn more about the complex way different schemes interact by comparing the response in other models. The approach used here is thus likely to be useful for other similar studies.

As pointed out in section 3a, there is a shift in precipitation from the convectively active regions to the less active regions, improving the climatology in some regions and degrading it in others. Changes in the climatological mean precipitation for the latitude band from  $5^{\circ}\text{S}$  to  $5^{\circ}\text{N}$  are shown in Fig. 13a together with various spinup terms associated with convective activ-

ity. Collins et al. (2001) show that in the aquaplanet version of HadAM3 there is less deep convection in the L30 model and more detrainment in the midtroposphere (see also Fig. 10). They point out that this pattern of convection looks more realistic than the purely deep or shallow convection in the L19 model. G. Martin (2000, personal communication) finds that the single-column version of HadAM3 exhibits similar behavior. The L30 models are better able to resolve the vertical structure around the freezing level. However, the response may not be entirely correct as the detrainment has unrealistic dependence on resolution. A similar response is seen in our results (Fig. 13c). Over South America ( $60^{\circ}\text{W}$ ) and southern Africa ( $30^{\circ}\text{E}$ ) and the Indonesian islands (e.g.,  $100^{\circ}\text{E}$ ) convective increments act to increase moisture in the midtroposphere consistent with enhanced detrainment. Stabilization of the midtroposphere through increased detrainment means that subsequent convection is not as deep on average in these regions, consistent with reduced precipitation. Reductions in convective activity locally will tend to be offset globally by increases in activity elsewhere and this is exactly what happens in the model. For example, northeast of the Indonesian islands there is increased precipitation (the top right-

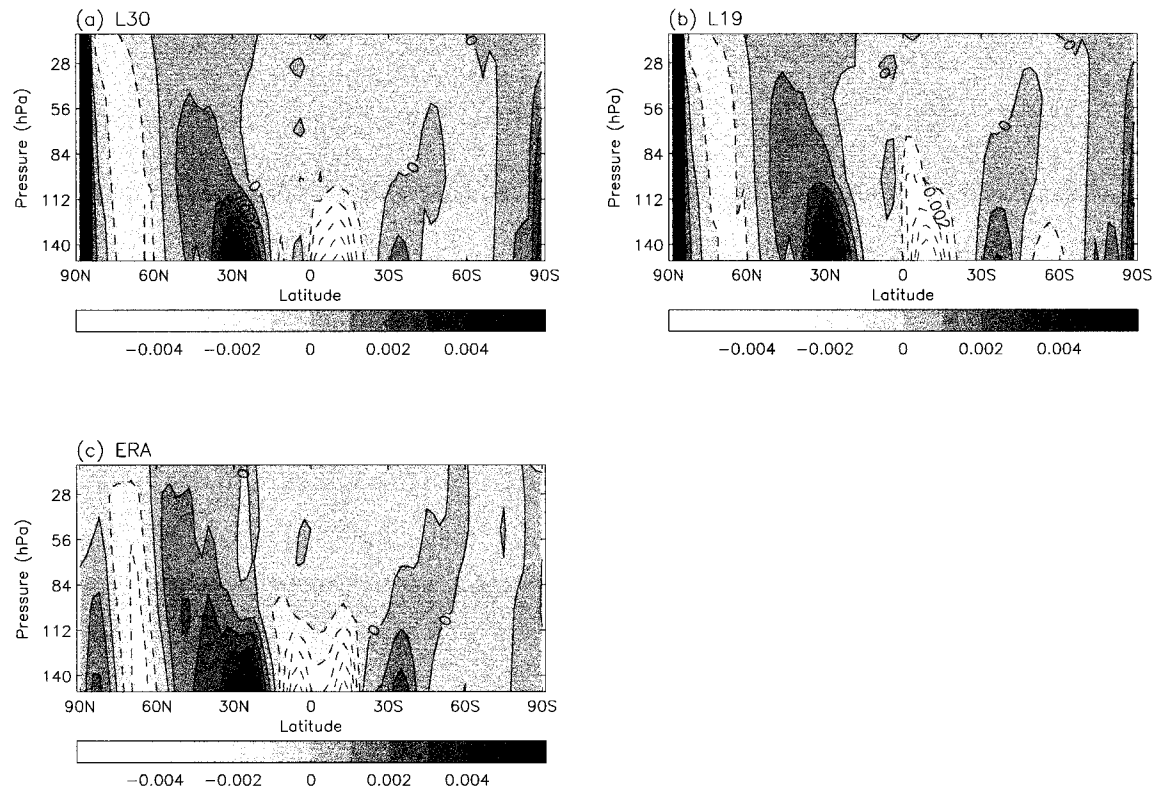


FIG. 11. Lat–pressure cross sections of zonal-mean vertical velocity from 150 to 10 hPa for (a) L30 ensemble mean, (b) L19 ensemble mean, and (c) ERA for the same time periods as used in Fig. 2. The contour interval is  $10^{-3} \text{ m s}^{-1}$ .

hand corner of Fig. 13a, see also the broader region of increased rainfall over the Pacific in Fig. 6b).

The changes in moisture distribution resulting from the changes in convective activity affect the formation of cloud. Figure 13b shows that more cloud forms in the midtroposphere where there is enhanced detrainment and less cloud forms in the upper troposphere, which is drier. This in turn impacts on the longwave cloud forcing. Longwave absorption is enhanced below the increased cloud (warming at 650 hPa) and emission is increased above (cooling at 550 hPa). There is also decreased longwave absorption in the upper troposphere consistent with the reduced cloud. The resulting increases in cooling above 600 hPa dominate the changes in the net heating terms in the spinup integrations (Fig. 9) leading to the increased cold bias in the tropical mid- and upper troposphere.

In summary, the tropical response to increasing vertical resolution has a mixed impact on model systematic errors. Improvements are indicated by  $\checkmark$ , degradations by  $\times$ , and neutral changes by  $\checkmark \times$  in the following.

1) There is more detrainment from convection in the midtroposphere. This may be partly due to better representation of vertical structure and partly due to unrealistic level dependence in the scheme. Precipitation decreases as there is less deep convection. ( $\checkmark \times$ )

- 2) Another impact of this is that more cloud forms in the midtroposphere and there is enhanced longwave cooling from the top of this cloud contributing to an increase in the model's cold bias. ( $\times$ )
- 3) Convection is more active over some tropical ocean areas giving increased precipitation. ( $\checkmark$ )
- 4) The upper troposphere is drier and less cloud forms there. There is correspondingly less longwave heating by clouds in the upper troposphere contributing further to the model's cold bias. ( $\times$ )
- 5) The net drying due to changes in convection dominates the model's moisture response (Figs. 10a and 10b) with the increased detrainment having little impact on the zonal mean moisture climatology (Figs. 10a and 10c). ( $\times$ )
- 6) The convective heating associated with these changes is swamped by relative longwave radiative cooling associated with the cloud changes (Figs. 9a and 9d). ( $\times$ )

The summary illustrates the nonlinearity of the model response. Convection is sensitive to resolution changes, both directly through the formulation of the scheme, and indirectly through its response to the resolved temperature and moisture profiles. The resulting changes in convective activity are responsible for the main changes in basic model fields in the Tropics. Some of these responses are direct, namely those of precipitation and

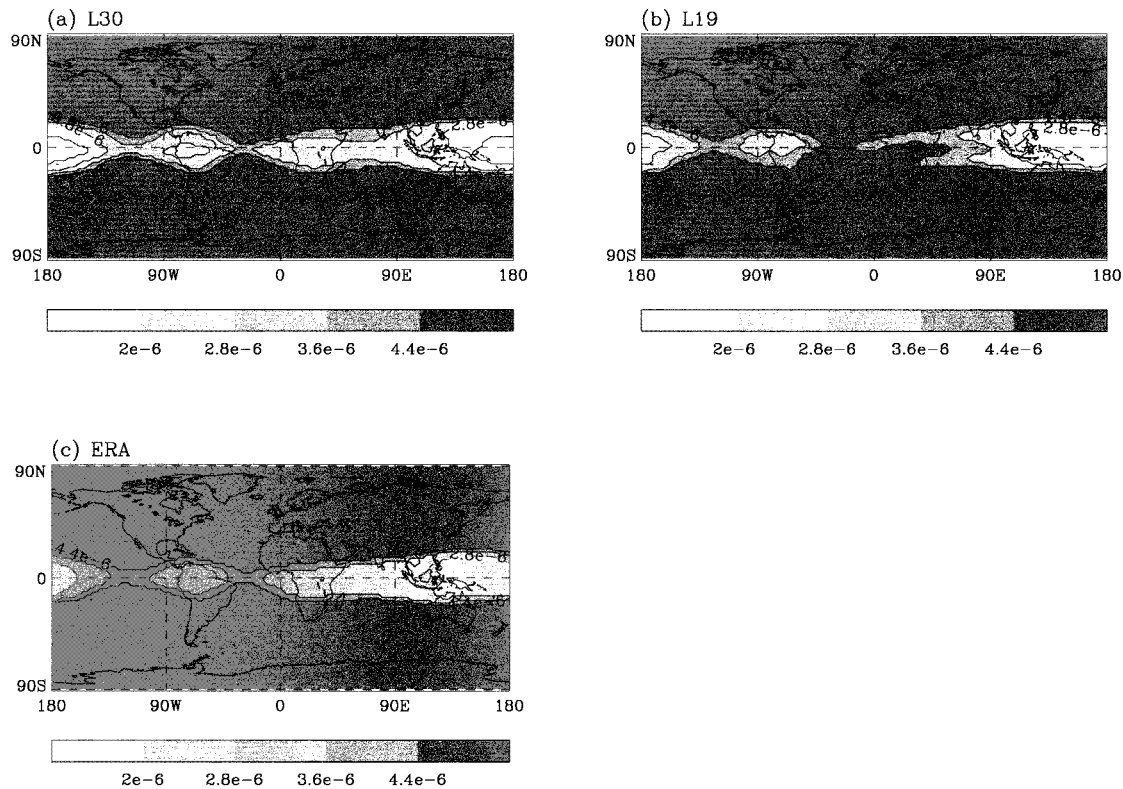


FIG. 12. As Fig. 7 but for saturation vapor pressure at 100 hPa plotted on a lat-long map. The contour interval is  $0.8 \times 10^{-6}$ .

moisture. Others are indirect; in particular temperature changes due to the impact of moisture changes on cloud formation and cloud radiative forcing.

### c. Water vapor and the radiative balance of the atmosphere

Water vapor feedback on radiation is one of the important processes determining the net impact of changes in greenhouse gases (Houghton et al. 1995). Consequently, it is important to model the processes involved accurately. The radiation scheme in HadAM3 (Edwards and Slingo 1996) represents all aspects of radiative transfer in the atmosphere better than schemes in earlier climate models. As we have already shown, there are a number of deficiencies in the model's representation of water vapor and the associated hydrological cycle. Some of these are improved by increasing vertical resolution, but others are not. This section focuses on the consequences of these changes for representing the clear-sky longwave radiation in the atmosphere.

Clear-sky longwave radiation (OLR<sub>c</sub>) is dependent on the temperature and water vapor content of the atmosphere and temperature at the earth's surface. Surface longwave emission is controlled strongly by the surface temperature. Water vapor affects OLR<sub>c</sub> by absorbing radiation from the surface and surrounding atmosphere and reemitting it at the local temperature. The atmo-

sphere is generally colder than the surface, so the absorption and reemission of longwave radiation by water vapor results in a lower value of OLR<sub>c</sub> than would be the case if the radiation were to pass directly from the surface to space. The changes in surface temperature and column water vapor and their impact on OLR<sub>c</sub> are summarized in Fig. 14. Figure 14a shows the 17-yr DJF mean of the top of atmosphere OLR<sub>c</sub> from the L30 model. Maxima in OLR<sub>c</sub> occur in the subtropical descending branches of the Hadley circulation where the relatively dry atmosphere allows much of the surface longwave radiation to escape to space. Lower values of OLR<sub>c</sub> occur in the relatively moist regions of the ITCZ near the equator and in the South Pacific convergence zone. On changing from 19 to 30 levels there are widespread increases in OLR<sub>c</sub> in the Tropics (Fig. 14b) associated with decreases in column water vapor (Fig. 14e)—notice that the red areas in Figs. 14b and 14e are well correlated. Local decreases in OLR<sub>c</sub> in the Tropics and subtropics are less obviously associated with increases in column water vapor, although there are correlations (blue areas) over the Persian Gulf and off the west coasts of Africa and South America. Outside the Tropics changes in OLR<sub>c</sub> are determined by changes in surface temperature (Fig. 14d). There are widespread large increases in surface temperature and OLR<sub>c</sub> (red) over northern Asia. However, variability is also large in this region during winter as surface temperatures are

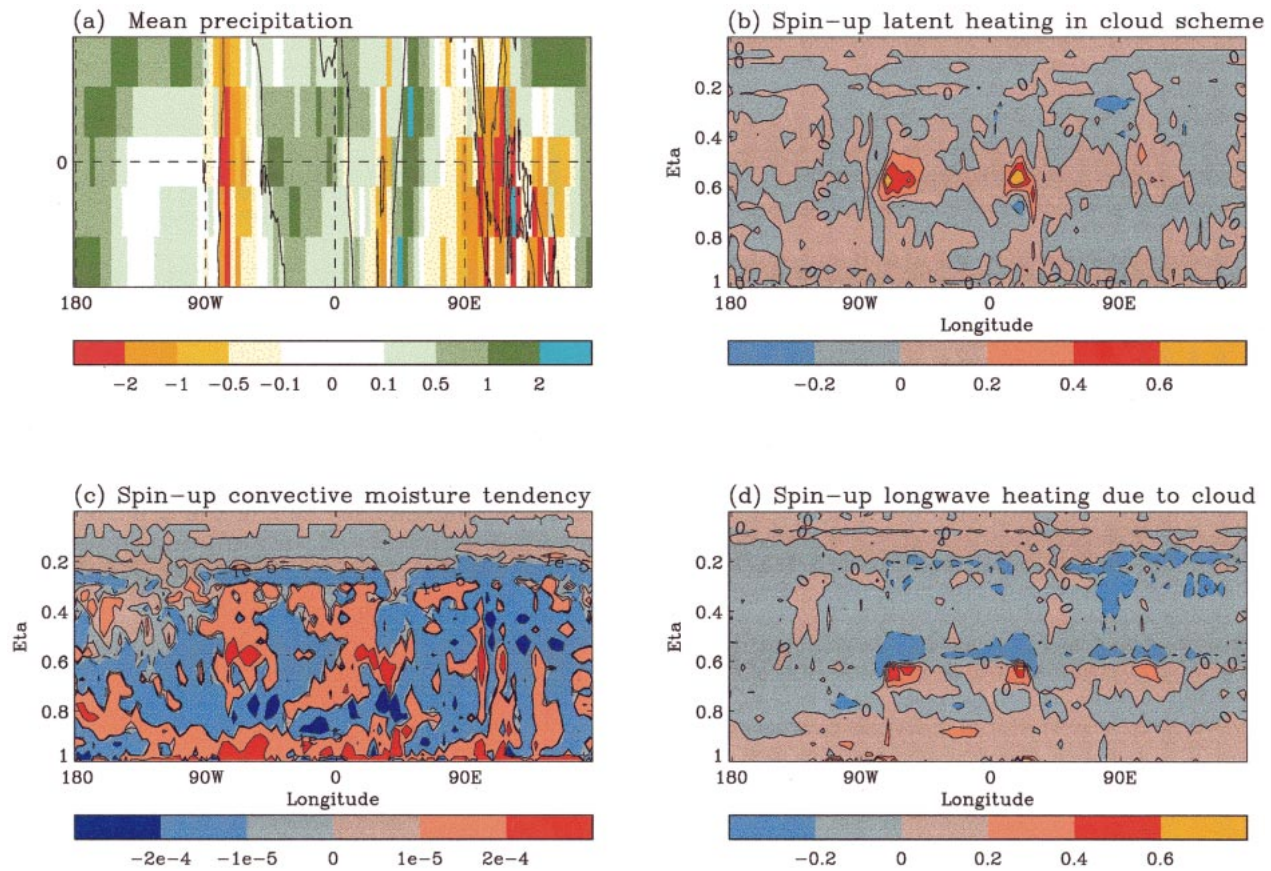


FIG. 13. (a) Lat-long map from 5°S to 5°N of precipitation differences between the L30 and L19 ensembles for the 17-yr DJF means from 1979 to 1995. The scale is the same as the one in Fig. 6. The rest of the panels are differences between two sets of ten 3-day spinup integrations, one set with 30 levels and the other with 19, both initialized from the same set of analyses. All plots are long-eta cross sections averaged between 5°S and 5°N. (b) Latent heating in the cloud scheme plotted with a contour interval of 0.2 K day<sup>-1</sup>. (c) Convective moisture tendency. The units are in kg kg<sup>-1</sup> and contours are  $2 \times 10^{-4}$ ,  $-10^{-5}$ , 0,  $10^{-6}$ ,  $10^{-5}$ ,  $2 \times 10^{-4}$ . (d) Longwave heating due to cloud scheme plotted with a contour interval of 0.2 K day<sup>-1</sup>.

strongly dependent on the circulation and cloud cover. Consequently, the statistical significance of the differences is small and only a small percentage of the changes show up in Fig. 14. Similar increases over Antarctica are significant.

Many of the changes in column water vapor lead to improvements in the simulation compared to ERA. This can be seen by comparing Figs. 14e and 14f—improvements arise where the plots have opposite colors and vice versa. In particular, the decreases in water vapor (colored red) over the Indian Ocean, southern Africa, South America, and the central Pacific off the coast of Central America are all improvements. The associated increases in OLRc (also colored red) lead to improved agreement between the model and ERBE—again comparing Figs. 14b and 14d improvements arise where plots have opposite colors. The decreases in column water vapor (colored red) over Indonesia worsen the simulation both in terms of column water vapor and the associated increases in OLRc. Despite the local improvements, the changes in zonal mean specific humid-

ity generally worsen the simulation (section 3a). The reason for this is that the local negative biases are not changed much, while the positive biases are reduced. Comparing Figs. 14b, c, and d at high northern latitudes, it is clear that the small regions of statistically significant increases in surface temperature at high northern latitudes have a mixed impact on OLRc. In the Antarctic, warmer surface temperatures in the L30 model (associated with circulation changes, Fig. 5) apparently worsen the simulation. Neither of these results are particularly conclusive since ERBE data are not reliable over ice (Harrison et al. 1990). Overall the global mean OLRc increases by  $1.1 \text{ W m}^{-2}$  reducing the global mean error to  $-5 \text{ W m}^{-2}$ .

## 5. Conclusions

We showed that 30 levels and a resolution of 25 hPa around the tropopause are sufficient in the Hadley Centre climate model to adequately resolve the tropopause and hygropause and the advection of temperature and

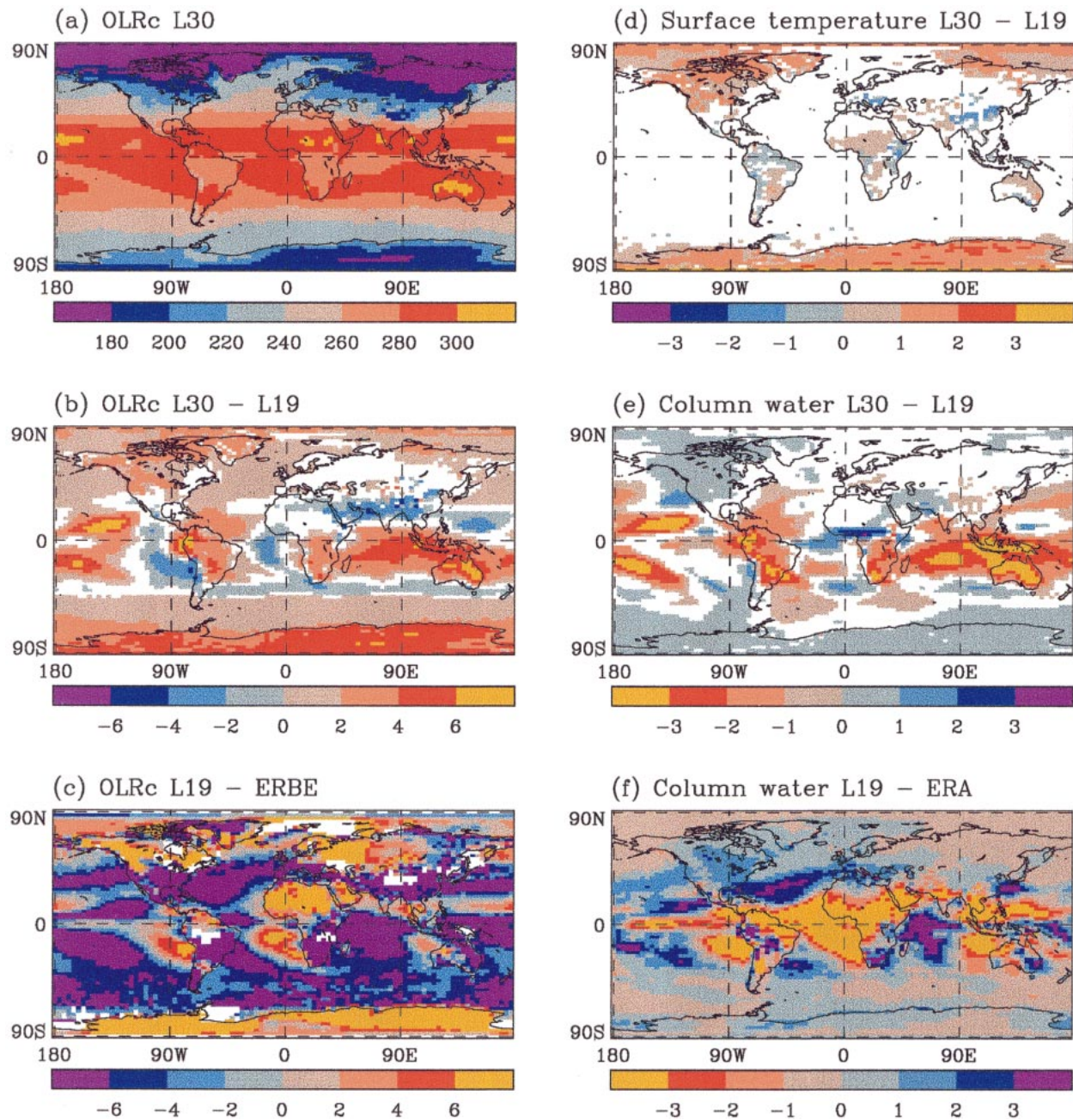


FIG. 14. Lat-long maps for the 17-yr DJF ensemble means from 1979 to 1995 for the following fields. (a) OLRc at the top of the atmosphere for L30. The contour interval is  $20 W m^{-2}$ . (b) As (a) but L30 - L19. The contour interval is  $2 W m^{-2}$ . (c) As (b) but L19 - ERBE. (d) Surface temperature differences between L30 and L19. The contour interval is 1 K. (e) Column water vapor differences between L30 and L19. The contour interval is  $1 kg m^{-2}$ . (f) As (e) but the difference between L19 and ERA. (b), (d), and (e) only show differences that are significant at the 95% confidence level.

moisture whereas 19 levels are not sufficient. We also showed that the model had sensitivities to resolution in the Tropics due to the way the model physical parameterizations, and in particular the convection scheme, are formulated. In summary, the main changes in climatology on increasing the vertical resolution of the model are as follows. Improvements are indicated by ticks and degradations by crosses; the main processes

contributing to the change are listed in brackets at the end.

- 1) Upper-tropospheric and stratospheric temperatures increase.  $\checkmark$  [dynamics, radiation]
- 2) Tropical temperatures decrease.  $\times$  [convection]
- 3) The westerly jets move equatorward and weaken.  $\times \checkmark$

- 4) Both specific and relative humidity decrease in the upper troposphere.  $\checkmark$  [dynamics]
- 5) Tropical humidities decrease improving the simulation locally, but worsening the zonal mean.  $\checkmark \times$  [convection]

The Eulerian advection in the model is unable to advect moisture or temperature accurately in the tropopause region with 19 levels, but does substantially better when 30 levels are used. The Met Office will shortly introduce a new model that replaces the Eulerian formulation of the dynamics with a semi-Lagrangian one. The smaller computational error of the semi-Lagrangian approach may lead to fewer inaccuracies in moisture advection near the tropopause. Results from other semi-Lagrangian models are encouraging. The ECHAM4 model (Roeckner et al. 1996) simulates upper-troposphere–lower-stratosphere water vapor reasonably well, even at relatively low vertical resolutions (Land et al. 1999), while the Goddard Earth Observing System semi-Lagrangian GCM (Chen and Bates 1996) simulates the polar tropopause region better than a corresponding Eulerian model.

Even with Eulerian advection the L30 model produces a very good simulation of temperature and moisture in the tropopause region. Our results compare well with the available observational and analysis datasets. We use ERA in the troposphere and HALOE in the stratosphere, since ERA does not include observations of water vapor in the stratosphere. The improvement in the moisture distribution is particularly striking in the lower stratosphere. At high levels in the 19-level model most of the moisture disappears, whereas in the 30-level model there is a reasonable distribution of moisture. The basic longitudinal structure of water vapor in the tropical lower stratosphere associated with regions of strong and weak convection is well reproduced in the model. High-latitude water vapor values are still too low, consistent with the fact that there is no chemical source of water vapor (through methane oxidation) in the model.

The reduction in the temperature bias in the extratropical upper troposphere is related to the reduction in the moisture bias in two ways. The improvement comes partly from the improved representation of advection and partly from the radiative feedback on the moisture changes. Our results contrast with those of Williamson and Olsen (1998) who find that the cold bias worsens at the polar tropopause in both the Eulerian and semi-Lagrangian versions of their model when they increase vertical resolution.

The response of water vapor and temperature in the tropical troposphere to increased vertical resolution illustrates the complex interaction between different physical parameterizations in the model. Changes in the behavior of convection with improved representation of the vertical structure of temperature and moisture lead to enhanced detrainment of moisture in the midtroposphere in some convectively active regions stabilizing

the midtroposphere so that subsequent convection is not as deep. Convective activity shifts to less active regions. The net effect of these changes on moisture is to moisten the midtroposphere and to dry the upper troposphere. Associated increases in cloud in the midtroposphere and decreases in the upper troposphere result in relatively more longwave cooling in the upper troposphere and an increased cold bias.

Other studies show a variety of responses of physical parameterizations to increases in vertical resolution. The responses depend on the details of the schemes used and the method of testing. Bushell and Martin (1999) show that increasing vertical resolution in the boundary layer in HadAM2b (an earlier version of the Hadley Centre model) leads to improved vertical structure in the boundary layer in a variety of situations. (Note: our experiments have little impact on the boundary layer, as the bottom three levels are unchanged between the L19 and L30 models.) However, they also find an underlying sensitivity to vertical resolution in model interactions between boundary layer and convection processes that appears unrealistic. Studies with other models (e.g., Williamson and Olsen 1998) indicate improved behavior of convective parameterizations with increased resolution. Tompkins and Emanuel (2000) show that the convection schemes they tested in their single-column model converged at a vertical resolution of 25 hPa. Work is in progress at the Met Office to reduce the sensitivity to resolution of the convection scheme used in HadAM3 and to improve its interaction with the boundary layer scheme.

Despite the problems of simulating water vapor in the Tropics, overall the L30 version of HadAM3 has an improved climatology. The improvements in the global hygropause structure are particularly striking. Even in the tropical troposphere, the L30 model reproduces many aspects of the water vapor structure and evolution and its interaction with clear-sky radiation. For example, reductions in column water locally and associated increases in OLRc improve the simulation even though they worsen the zonal mean response.

*Acknowledgments.* This work was carried out under the Public Meteorological Services Research programme of The Met Office and contract PECD 7/12/37 funded by the U.K. Department of the Environment, Transport and the Regions. We thank Gill Martin for helpful discussions and comments on the first draft of this paper, Simon Wilson for help with the figures, Dave Sexton for advice on the most appropriate statistical tests to use, and anonymous reviewers for their constructive comments. We also thank ECMWF and the HALOE project and science teams for the use of ERA and HALOE datasets, respectively. The HALOE data were obtained via the British Atmospheric Data Centre.

## APPENDIX A

## Summary of HadAM3 Model Formulation

Process	Description	References
Dynamics	The current UM is a hydrostatic, gridpoint model using an Arakawa B grid and hybrid vertical coordinates. It uses an Eulerian advection scheme. Both integrations use a $2.5^\circ \text{ lat} \times 3.75^\circ \text{ long}$ grid and a 30-min time step.	Cullen (1993); Cullen and Davies (1991)
Radiation	The scheme has six shortwave bands and eight longwave bands. It includes the effects of $\text{CO}_2$ , $\text{H}_2\text{O}$ , $\text{O}_3$ , $\text{O}_2$ , $\text{N}_2\text{O}$ , $\text{CH}_4$ , CFC11, and CFC12. The model uses trace gas values appropriate for the AMIP2 period, i.e., 1979–1995. It also includes the effects of background aerosols.	Edwards and Slingo (1996) and modified by Cusack et al. (1999). Aerosol effects Cusack et al. (1998)
Clouds	The prognostic cloud scheme diagnoses cloud ice, cloud water, and cloud amount from the primary model variables $q_T$ (total moisture) and liquid water potential temperature.	Smith (1990) and modified by Gregory and Morris (1996)
Precipitation	Large-scale precipitation forms in association with stratiform cloud.	Senior and Mitchell (1993); Gregory (1995)
Convection	Moist and dry convection are modeled using the penetrative mass-flux scheme with the addition of convective downdrafts.	Gregory and Rowntree (1990); Gregory and Allen (1991)
Gravity wave drag	Orographic gravity wave drag	Gregory et al. (1998)
Boundary layer	Local mixing scheme	Smith (1990, 1993)
Convective momentum transport	The direct impact of convection on horizontal momentum	Gregory et al. (1997)
Land surface	Met Office Surface Exchange Scheme	Cox et al. (1999)
Sea surface temperature	Monthly mean sea surface temperatures and sea ice	Fiorino (1996)
Ozone	Lat–pressure monthly climatology	Wang et al. (1995)

## APPENDIX B

## Testing for Statistical Significance

The statistical significance of differences between the L30 and L19 ensemble means is assessed by performing a two-sample  $t$  test. The  $T$  statistic is calculated as follows:

$$T = (m_{30} - m_{19}) / (s_{30}^2/n_{30}n_{\text{yr}} + s_{19}^2/n_{19}n_{\text{yr}})^{1/2}, \quad (\text{B1})$$

$m_{30}$  and  $m_{19}$  are the time mean ensemble means of the L30 and L19 fields, respectively;  $s_{30}^2/n_{30}n_{\text{yr}}$  and  $s_{19}^2/n_{19}n_{\text{yr}}$  are the corresponding variances;  $n_{30}$  and  $n_{19}$  are the number of GCM integrations in the L30 and L19 ensembles, and  $n_{\text{yr}}$  is the number of years (i.e., 17) run for each ensemble member.

The time mean ensemble means are calculated in the usual way:

$$m = 1/(n_{\text{yr}}n_{\text{ens}}) \sum_{j=1}^{n_{\text{ens}}} \sum_{i=1}^{n_{\text{yr}}} x_{ij} \quad (\text{B2})$$

$n_{\text{ens}}$  is the number of ensemble members,  $x_{ij}$  is any field at either a single model grid point or a zonal mean.

Here  $s_{30}^2$  and  $s_{19}^2$  are estimates of the internal variance of each ensemble at any one point (or zonal mean). They are obtained by performing a one-way analysis of variance on each ensemble, following the method of Rowell et al. (1995). The variances of the time mean ensemble means are then the internal variances divided by the number of ensemble members and the number of years in each run.

Some fields may be affected by significant autocor-

relation, in which case  $s_{30}^2$  and  $s_{19}^2$  may be underestimated. The amount of autocorrelation between the  $x_{ij}$  is estimated as follows. The pooled lag  $-1$  correlation coefficient,  $\alpha$ , of deviations of the ensemble members from the ensemble mean is found. A  $t$  test is then performed to see if  $\alpha$  is significant as some correlation would be expected by chance. If the autocorrelation is significant then the Eq. (B1) must be modified as follows:

$$T = (m_{30} - m_{19}) / (s_{30}^2 a_{30} / n_{30} n_{\text{yr}} + s_{19}^2 a_{19} / n_{19} n_{\text{yr}})^{1/2}, \quad (\text{B3})$$

where  $a_{\text{ens}} = [1 + |(\alpha_{\text{ens}})|] / [1 - |(\alpha_{\text{ens}})|]$ . This increases the estimate of internal variance. The only fields affected are zonal-mean specific humidity in the stratosphere.

Finally  $T$  obtained from Eqs. (B1) or (B3) as appropriate is compared with a standard  $t$  distribution (in a two-tailed test) to determine whether  $m_{30}$  and  $m_{19}$  are different at the 95% significance level. Only significant differences are plotted in the figures. Note that we use the method outlined by Kanji (1994) to determine the appropriate number of degrees of freedom for the  $t$  distribution used in the  $t$  test:

Degrees of freedom

$$= \{(s_{30}^2/ne_{30} + s_{19}^2/ne_{19})^2 \div s_{30}^4/[ne_{30}^2(ne_{30} + 1)] + s_{19}^4/[ne_{19}^2(ne_{19} + 1)]\} - 2,$$

where  $ne_{\text{ens}} = n_{\text{yr}}n_{\text{ens}}/a_{\text{ens}=1}$ . This allows for the possibility of unequal variances in the L19 and L30 ensembles.

## REFERENCES

- Annamalai, H., J. M. Slingo, K. R. Sperber, and K. Hodges, 1999: The mean evolution and variability of the Asian summer monsoon: Comparison of ECMWF and NCEP/NCAR reanalyses. *Mon. Wea. Rev.*, **127**, 1157–1186.
- Baer, F., and Y. Zhu, 1992: Forecast accuracy with optimum vertical model truncation. *Mon. Wea. Rev.*, **120**, 2579–2591.
- Boville, B. A., 1991: Sensitivity of simulated climate to model resolution. *J. Climate*, **4**, 469–485.
- Bushell, A. C., and G. M. Martin, 1999: The impact of vertical resolution upon GCM simulations of marine stratocumulus. *Climate Dyn.*, **15**, 293–318.
- Chen, M., and J. R. Bates, 1996: A comparison of climate simulations from a semi-Lagrangian and an Eulerian GCM. *J. Climate*, **9**, 1126–1148.
- Collins, M., S. F. B. Tett, and C. Cooper, 2001: The internal climate variability of a version of the Hadley Centre coupled model without flux adjustments. *Climate Dyn.*, **17**, 61–81.
- Cox, P., R. Betts, C. Bunton, R. Essery, P. R. Rowntree, and J. Smith, 1999: The impact of new land surface physics on the GCM simulation of climate and climate sensitivity. *Climate Dyn.*, **15**, 183–203.
- Cullen, M., 1993: The unified forecast/climate model. *Meteor. Mag.*, **122**, 81–94.
- , and T. Davies, 1991: A conservative split explicit integration scheme with fourth order horizontal advection. *Quart. J. Roy. Meteor. Soc.*, **117**, 993–1002.
- Cusack, S., A. Slingo, J. M. Edwards, and M. Wild, 1998: The radiative impact of a simple aerosol climatology on the Hadley Centre Atmospheric GCM. *Quart. J. Roy. Meteor. Soc.*, **124**, 2517–2526.
- , J. M. Edwards, and J. M. Crowther, 1999: Investigating k-distribution methods for parameterising gaseous absorption in the Hadley Centre climate model. *J. Geophys. Res.*, **104**, 2051–2057.
- Edwards, J. M., and A. Slingo, 1996: Studies with a flexible new radiation code. I: Choosing a configuration for a large-scale model. *Quart. J. Roy. Meteor. Soc.*, **122**, 689–719.
- Fiorino, M., cited 1996: The AMIP boundary conditions. PCMDI report. [Available online at <http://www-pcmdi.llnl.gov/amip//AMIP2EXPDSN/BCS/bcsintro.html>]
- Gibson, J. K., P. Kallberg, S. Uppala, A. Hernandez, A. Nomura, and E. Serrano, 1997: *ERA Description*. ECMWF Re-Analysis Project Series, Vol. 1, ECMWF, 72 pp.
- Gleckler, P., Ed., cited 1996: AMIP newsletter No. 8. [Available online at <http://www-pcmdi.llnl.gov/amipnews.html>]
- Gregory, D., 1995: A consistent treatment of the evaporation of rain and snow for use in large-scale models. *Mon. Wea. Rev.*, **123**, 2716–2732.
- , and P. Rowntree, 1990: A mass flux convection scheme with representation of cloud ensemble characteristics and stability dependent closure. *Mon. Wea. Rev.*, **118**, 1483–1506.
- , and S. Allen, 1991: The effect of convective scale downdrafts upon NWP and climate simulations. Preprints, *Ninth Conf. on Numerical Weather Prediction*, Denver, CO, Amer. Meteor. Soc., 122–123.
- , and D. Morris, 1996: The sensitivity of climate simulations to the specification of mixed phase clouds. *Climate Dyn.*, **12**, 641–651.
- , R. Kershaw, and P. M. Inness, 1997: Parametrization of momentum transport by convection. II: Tests in single-column and general circulation models. *Quart. J. Roy. Meteor. Soc.*, **123**, 1153–1183.
- , G. J. Shutts, and J. R. Mitchell, 1998: A new gravity-wave-drag scheme incorporating anisotropic orography and low-level wave breaking: Impact upon the climate of the UK Meteorological Office Unified Model. *Quart. J. Roy. Meteor. Soc.*, **124**, 463–494.
- Harries, J. E., and Coauthors, 1996: Validation of measurements of water vapour from the Halogen Occultation Experiment, HALOE. *J. Geophys. Res.*, **101**, 10 205–10 216.
- Harrison, E. F., P. Minnis, B. R. Barkstrom, V. Ramanathan, R. D. Cess, and G. G. Gibson, 1990: Seasonal variation of cloud radiative forcing derived from the Earth Radiation Budget Experiment. *J. Geophys. Res.*, **95**, 18 687–18 703.
- Houghton, J. T., and Coauthors, 1995: *Climate Change 1994: Radiative Forcing of Climate Change and an Evaluation of the IPCC IS92 Emissions Scenarios*. Cambridge University Press, 572 pp.
- Inness, P. M., J. M. Slingo, S. J. Woolnough, R. B. Neale, and V. D. Pope, 2001: Organisation of tropical convection in a GCM with varying vertical resolution; Implications for the simulation of the Madden-Julian oscillation. *Climate Dyn.*, in press.
- Jackson, D. R., S. J. Driscoll, E. J. Highwood, J. E. Harries, and J. M. Russell III, 1998: Troposphere to stratosphere transport at low latitudes as studied using HALOE observations of water vapour 1992–1997. *Quart. J. Roy. Meteor. Soc.*, **124**, 169–192.
- Ji, M., and F. Baer, 1992: Three-dimensional scaling and consistent truncation of global atmospheric models. *Mon. Wea. Rev.*, **120**, 131–148.
- Kallberg, P., 1997: *Aspects of the Re-Analysed Climate*. ECMWF Re-Analysis Project Series, Vol. 2, ECMWF, 89 pp.
- Kanji, G. K., 1994: *100 Statistical Tests*. Sage Publications, 216 pp.
- Land, C., M. Ponater, R. Sausen, and E. Roeckner, 1999: The ECHAM4/L39(DLR) atmosphere GCM: Technical description and model climatology. DLR-Forschungsbericht, Vol. 31, 45 pp.
- Lane, D., R. Somerville, and S. Iacobellis, 2000: Sensitivity of cloud and radiation parameterizations to changes in vertical resolution. *J. Climate*, **13**, 915–922.
- Lindzen, R. S., and M. Fox-Rabinovitz, 1989: Consistent vertical and horizontal resolution. *Mon. Wea. Rev.*, **117**, 2575–2583.
- Mahlman, G., and L. J. Umshied, 1987: Comprehensive modelling of the middle atmosphere: The influence of horizontal resolution. *Transport Processes in the Middle Atmosphere*, G. Visconti and R. Garcia, Eds., D. Reidel, 251–266.
- Martin, G., 1999: The simulation of the Asian Summer Monsoon, and its sensitivity to horizontal resolution, in the UK Meteorological Office Unified Model. *Quart. J. Roy. Meteor. Soc.*, **125**, 1499–1525.
- , M. R. Bush, A. R. Brown, A. P. Lock, and R. N. B. Smith, 2000: A new boundary layer mixing scheme. Part II: Tests in climate and mesoscale models. *Mon. Wea. Rev.*, **128**, 3200–3217.
- McNally, A. P., and M. Vesperini, 1996: Variational analysis of humidity information from TOVS radiances. *Quart. J. Roy. Meteor. Soc.*, **122**, 1521–1544.
- Milton, S. F., S. J. Lorrimer, and B. V. Chalcraft, 1998: Parallel trials of enhanced vertical and horizontal resolution in the global Unified Model. The Met Office Forecasting Research Division Tech. Rep. 230, 77 pp.
- Nigam, S., I. M. Held, and S. W. Lions, 1986: Linear simulation of the stationary eddies in a general circulation model. *J. Atmos. Sci.*, **43**, 2944–2966.
- Ovarlez, J., and P. van Velthoven, 1997: Comparison of water vapor measurements with data retrieved from ECMWF analyses during the POLINAT experiment. *J. Appl. Meteor.*, **36**, 1329–1335.
- Peixoto, J. P., and A. H. Oort, 1996: The climatology of relative humidity in the atmosphere. *J. Climate*, **9**, 3443–3463.
- Pope, V. D., M. Gallani, P. R. Rowntree, and R. A. Stratton, 2000: The impact of new physical parametrizations in the Hadley Centre climate model—HadAM3. *Climate Dyn.*, **16**, 123–146.
- Randel, D. L., T. H. Vonder Haar, M. A. Ringerud, G. L. Stephens, T. J. Greenwald, and C. L. Combs, 1996: A new global water vapor dataset. *Bull. Amer. Meteor. Soc.*, **77**, 1233–1246.
- Roeckner, E., and Coauthors, 1996: The atmospheric general circulation model ECHAM-4: Model description and simulation of present-day climate. Max-Planck-Institut für Meteorologie Rep. 218, 90 pp.
- Rowell, D. P., 1998: Assessing potential seasonal predictability with

- an ensemble of multi-decadal GCM simulations. *J. Climate*, **11**, 109–120.
- , C. K. Folland, K. Maskell, and M. N. Ward, 1995: Variability of summer rainfall over tropical North Africa (1906–92): Observations and modelling. *Quart. J. Roy. Meteor. Soc.*, **121**, 669–704.
- Russell, J. M., and Coauthors, 1993: The Halogen Occultation Experiment. *J. Geophys. Res.*, **98**, 10 777–10 797.
- Senior, C. A., and J. F. B. Mitchell, 1993: CO<sub>2</sub> and climate: The impact of cloud parameterization. *J. Climate*, **6**, 393–418.
- Simmons, A. J., A. Untch, C. Jakob, P. Kallberg, and P. Unden, 1999: Stratospheric water vapour and tropical tropopause temperatures in ECMWF analyses and multi-year simulations. *Quart. J. Roy. Meteor. Soc.*, **125**, 353–386.
- Smith, R. N. B., 1990: A scheme for predicting layer clouds and their water content in a general circulation model. *Quart. J. Roy. Meteor. Soc.*, **116**, 435–460.
- , 1993: Experience and developments with the layer cloud and boundary layer mixing schemes in the UK Meteorological Office Unified Model. *Proc. of the ECMWF/GCSS Workshop on Parameterization of the Cloud-Topped Boundary Layer*, ECMWF, Reading, United Kingdom, 319–339.
- Stone, E. M., L. Pan, B. Sandor, W. G. Read, and J. W. Waters, 2000: Spatial distributions of upper tropospheric water vapor measurements from the UARS Microwave Limb Sounder. *J. Geophys. Res.*, **105**, 12 149–12 161.
- Stratton, R. A., 1999: A high resolution AMIP integration using the Hadley Centre model HadAM2b. *Climate Dyn.*, **15**, 9–28.
- Thompson, D. W. J., and J. M. Wallace, 2000: Annular modes in the extratropical circulation. Part I: Month-to-month variability. *J. Climate*, **13**, 1000–1016.
- Tompkins, A. M., and K. A. Emanuel, 2000: The vertical resolution sensitivity of simulated equilibrium temperature and water vapour profiles. *Quart. J. Roy. Meteor. Soc.*, **126**, 1219–1238.
- Wang, W.-C., X.-Z. Liang, D. Dudek, D. Pollard, and S. L. Thompson, 1995: Atmospheric ozone as a climate gas. *Atmos. Res.*, **37**, 247–256.
- Williamson, D. L., and J. G. Olsen, 1998: A comparison of semi-Lagrangian and Eulerian polar climate simulations. *Mon. Wea. Rev.*, **126**, 991–1000.
- , —, and B. A. Boville, 1998: A comparison of semi-Lagrangian and Eulerian tropical climate simulations. *Mon. Wea. Rev.*, **126**, 1001–1012.
- Wilson, D. R., and S. P. Ballard, 1999: A microphysically based precipitation scheme for the Meteorological Office Unified Model. *Quart. J. Roy. Meteor. Soc.*, **125**, 1607–1636.
- WMO, 1987: Numerical weather prediction: Progress report for 1986. *WMO Bulletin*, Vol. 186, 257 pp.
- Xie, P., and P. A. Arkin, 1997: Global precipitation: A 17-year monthly analysis based on gauge observations, satellite estimates, and numerical model outputs. *Bull. Amer. Meteor. Soc.*, **78**, 2539–2558.